Achieving Effective Terminal Exciton Delivery in Quantum Dot Antenna-Sensitized Multistep DNA Photonic Wires

Christopher M. Spillmann,[†,●] Mario G. Ancona,[‡,●] Susan Buckhout-White,[†,⊥] W. Russ Algar,[†,⊥,▽] Michael H. Stewart,[§] Kimihiro Susumu,[§,¶] Alan L. Huston,[§] Ellen R. Goldman,[†] and Igor L. Medintz[†,*]

[†]Center for Bio/Molecular Science and Engineering, Code 6900, [‡]Electronic Science and Technology Division, Code 6876, and [§]Optical Sciences Division, Code 5611, U.S. Naval Research Laboratory, Washington, D.C. 20375, United States, [⊥]College of Science, George Mason University, Fairfax, Virginia 22030, United States, and [¶]Sotera Defense Solutions, Annapolis Junction, Maryland 20701, United States. [●]C.M.S. and M.G.A. contributed equally to this work. [▽]Present address: W.R.A.: Department of Chemistry University of British Columbia, Vancouver, BC V6T 1Z1.

ABSTRACT Assembling DNA-based photonic wires around semiconductor quantum dots (QDs) creates optically active hybrid architectures that exploit the unique properties of both components. DNA hybridization allows positioning of multiple, carefully arranged fluorophores that can engage in sequential energy transfer steps while the QDs provide a superior energy harvesting antenna capacity that drives a Förster resonance energy transfer (FRET) cascade through the structures. Although the first generation of these composites demonstrated four-sequential energy transfer steps across a distance >150 Å, the exciton transfer efficiency reaching the final, terminal dye was estimated to be only ~0.7% with no concomitant sensitized emission observed. Had the terminal Cy7 dye utilized in that construct provided a sensitized emission, we estimate that this would have equated to an overall end-to-end ET efficiency of ≤0.1%. In this report, we demonstrate that overall energy flow through a second generation hybrid architecture can be significantly improved by reengineering four key aspects of the composite structure: (1) making the initial DNA modification chemistry smaller and more facile to implement, (2) optimizing donor–acceptor dye pairings, (3) varying donor–acceptor dye spacing as a function of the Förster distance R_0, and (4) increasing the number of DNA wires displayed around each central QD donor. These cumulative changes lead to a *2 orders of magnitude* improvement in the exciton transfer efficiency to the final terminal dye in comparison to the first-generation construct. The overall end-to-end efficiency through the optimized, five-fluorophore/four-step cascaded energy transfer system now approaches 10%. The results are analyzed using Förster theory with various sources of randomness accounted for by averaging over ensembles of modeled constructs. Fits to the spectra suggest near-ideal behavior when the photonic wires have two sequential acceptor dyes (Cy3 and Cy3.5) and exciton transfer efficiencies approaching 100% are seen when the dye spacings are 0.5 × R_0. However, as additional dyes are included in each wire, strong nonidealities appear that are suspected to arise predominantly from the poor photophysical performance of the last two acceptor dyes (Cy5 and Cy5.5). The results are discussed in the context of improving exciton transfer efficiency along photonic wires and the contributions these architectures can make to understanding multistep FRET processes.

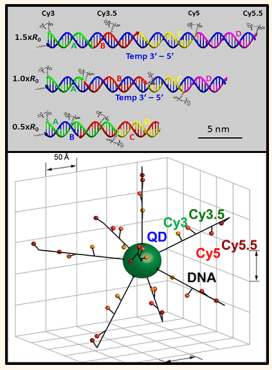

KEYWORDS: semiconductor nanocrystal · quantum dot · sensitization · dye · fluorophore · photonic wire · antenna · self-assembly · DNA · FRET · nanotechnology · energy transfer · exciton

The growing versatility of DNA-based architectures is providing unique opportunities for research into new nanoscale structures and functional devices.[1−4] An ever-expanding variety of designer DNA structures have been reported and applications under investigation include molecular scale electronics, molecular motors, biocomputing, biosensing, drug delivery, optical coding, and chemical synthesis.[1−10] The wide-ranging utility of these "nanoplatforms" arises directly from the unique physicochemical properties of DNA, its ability to noncovalently self-assemble into complex yet predictable 1-, 2-, or 3-dimensional structures, and easy access to building-block oligomeric components *via* customizable, automated synthetic chemistry that allows for multiple site-specific chemical modifications.[1,4,6,7,10−14]

* Address correspondence to Igor.medintz@nrl.navy.mil.

Received for review May 15, 2013 and accepted June 26, 2013.

Published online July 11, 2013
10.1021/nn402468t

One growing area where DNA architectures have great promise is that of photonic wires and photonic networks. In these structures, the DNA scaffolding is decorated with chromophores in such a manner that the dipolar fields of the latter interact with each other.[5,6,12,15−17] Although plasmonically active DNA wires have been described and are actively researched,[4,18,19] Förster resonance energy transfer (FRET) is the most common photophysical process currently investigated within these structures. Given the capacity for individual control of fluorophore placement in 3-D structures, FRET-based DNA photonic networks are especially relevant for understanding and optimizing energy harvesting and transport at the nanoscale in the pursuit of matching the efficiency of natural light harvesters.[3,5,6,12,15,16,20] The ability to incorporate not only standard organic dyes into these structures, but also fluorescent nanoparticles, metal-cryptates, and fluorescent proteins, is expected to enhance their energy transfer (ET) capabilities, especially within the context of multistep FRET cascades.[17,21]

Among the widely diverse family of available fluorescent materials, luminescent semiconductor quantum dots (QDs) appear to have much to offer as energy harvesting antenna and initial sensitizers for photonic wires and networks.[22] Attractive properties of QDs within this context include the following abilities: (1) to be excited at one wavelength far removed from their discrete, narrow photoluminescence (PL); (2) to minimize direct acceptor excitation; (3) to optimize spectral overlap by pairing QD PL with acceptor(s) absorption; and (4) to create structures in which multiacceptor photonic wires are arranged concentrically around the QD, thus proportionally increasing the FRET acceptor cross section and, in turn, the potentially accessible FRET efficiency.[22,23]

Reflecting the growing interest in construction of complex photonic networks, there have been several recent reports of increasingly complex DNA-based photonic networks, many incorporating diverse fluorophore materials including QDs and other nanoparticles.[17,24,25] For example, Niemeyer's group assembled a fluorescent protein−DNA dye construct onto a QD which provided for multistep ET over distances approaching 130 Å.[26] With single molecule precision, Tinnefeld's group showed that the positioning of individual dyes, in particular an intermediary relay dye, on a DNA origami scaffold could spatially direct the ET to a desired acceptor.[20] Albinsson's group recently reported a DNA structure that was intercalated with YO-PRO-1 dye and funneled energy by homoFRET to a porphyrin complex.[27] Graugnard and co-workers utilized a toehold-mediated strand invasion of a three-dye construct to demonstrate exciton-based Boolean logic elements.[5] Liu's lab assembled seven-helix DNA bundles into cyclic arrays that displayed three distinct chromophores to approximate a natural photosynthetic system.[12] In another elegant example, Tikhomirov *et al.* synthesized QDs using thiol-modified DNA strands and then exploited their complementarity to assemble hierarchical structures allowing differentially sized QDs to transfer energy sequentially.[28]

We previously investigated multifluorophore DNA−photonic wires self-assembled around central QD scaffolds for their unique energy-harvesting and exciton transfer properties.[29] Within this architecture, the QD functioned as an ultraviolet absorbing donor that initiated a FRET cascade through sequentially red-shifted acceptor-dyes linearly arranged on the DNA. The ability to rapidly reconfigure the structure by altering the DNA design allowed multiple characteristics to be investigated, including the use of various dyes at different positions along the DNA and use of intercalating dyes that engaged in homoFRET. This study culminated in a nanostructure of approximately 360 Å in diameter, with ∼4 DNA wires displayed around each QD, where each wire was hybridized to 4-sequentially arranged acceptor dyes that engaged in 4 consecutive ET steps. Tracking the ET efficiency through this final structure revealed that only ∼0.7% of the excitation energy was being delivered to the terminal Cy7 acceptor dye. Furthermore, the Cy7 acted as a dark quencher and did not exhibit detectable FRET-sensitized emission. On the basis of the reported quantum yield, QY, of Cy7 (∼0.28) and the cumulative efficiency of the previous ET steps, *if* the terminal Cy7 had provided sensitized emission, we estimate that this would have equated to an overall end-to-end ET efficiency of ≤0.1%. Clearly, this photonic wire design and, indeed, many other similar constructs[4−6,12,15,16,21,28] would benefit from increasing the exciton flow/FRET efficiency within and through the system.

Here, we seek to improve FRET efficiency in QD−DNA constructs structurally analogous to our first-generation photonic wires by re-engineering four key aspects: (1) making the initial DNA modification chemistry more facile to implement and smaller in extension/separation; (2) optimizing donor−acceptor dye pairings; (3) varying donor−acceptor dye spacing as a function of the Förster distance, R_0; and (4) controllably increasing the number of DNA wires displayed around each central QD donor. A schematic of the current construct highlighting some of these variables (in red) along with the assembly chemistry is shown in Figure 1. We find that the changes in design cumulatively lead to improvement in the exciton transfer efficiency to the terminal dye by *2 orders of magnitude* compared to the first generation of structures. The overall end-to-end efficiency through the optimized, cascaded five-fluorophore/four-ET step system now approaches 10%. We also find that, as expected, the multiple photophysical processes underpinning the behavior of the QD-photonic wire systems are quite complex. In addition to the ensemble nature of the samples, complicating factors include variable

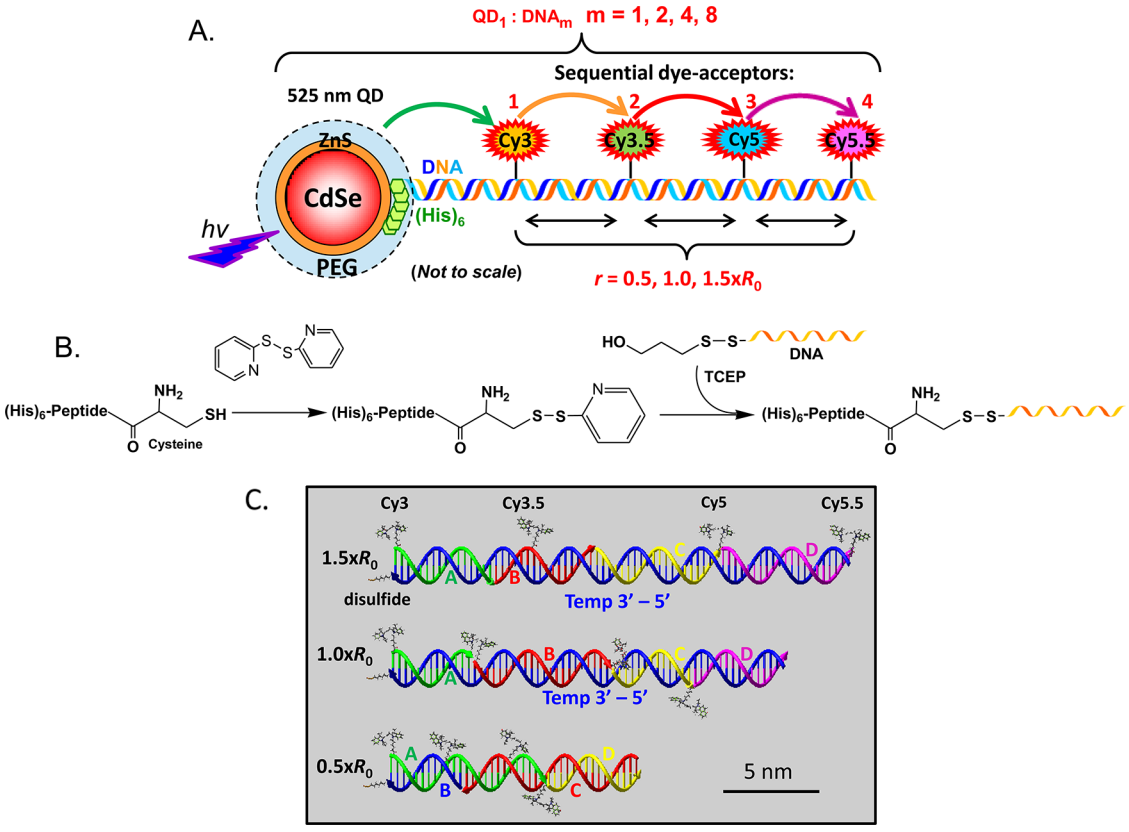

Figure 1. Schematic of the DNA–peptide linkage chemistry and the QD–DNA structures. (A) Schematic of a central QD donor assembled with a peptide–DNA photonic wire by $(His)_6$-metal affinity coordination; only one wire is shown for clarity. Pertinent characteristics examined in these structures include the use of new dye pairs, the interfluorophore distances, which are varied as a function of 0.5×, 1.0×, and 1.5 × R_0 along with the number of arms displayed around the QD, which are doubled incrementally from 1 to 8. These variables are highlighted in red. (B) The terminal cysteine on a $(His)_6$-appended peptide is activated with pyridine disulfide to form a pyridyl disulfide that then undergoes thiol-exchange to the DNA which has been reduced with TCEP to link the peptide to the thiolated DNA. The $(His)_6$-motif is used to purify the peptide–DNA conjugate with Ni^{2+}-affinity media and for subsequent assembly to the QDs. (C) Schematic showing the DNA portion of the hybrid wire, the location of the individual DNA sequences making up each wire, and the location of the dyes in each structure relative to each other and the QD which would be to the left of each DNA complex. The disulfide linker joining the DNA to the peptide is also shown. Note, the relative size scale.

numbers of wires per QD, flexibility of the dye linkers, potential subpopulations of incompletely formed structures, photobleached/inactive dyes, and other nonidealities. To address this complexity, we employ two different analytical approaches to aid in interpreting the underlying exciton transfer properties: one approach is empirical in nature while the other is based on Förster theory. Although neither analysis can be regarded as definitive, their combined insight allows us to develop an understanding of the complex photophysics in our QD-photonic wire constructs, to better estimate the exciton transfer efficiencies, to identify sources of inefficiency, and to suggest avenues for further improving the overall performance of the photonic wires.

RESULTS AND DISCUSSION

DNA Sequences, Peptide Modification, Ratiometric Coordination to QDs and Controlled Fluorophore Spacing. A detailed description of all the materials and synthetic procedures used along with the wire assembly protocols can be found in the Materials and Methods and Supporting Information (SI) sections. This study required QD interactions with four sequentially placed dye acceptors linearly arrayed on a DNA duplex that extended outward from the QD surface. The number of dye-labeled DNA molecules per QD (i.e., the valency) and the spacings between the dyes also had to be amenable to further manipulation, see Figure 1A. To accomplish this, we again utilized hexahistidine or $(His)_6$-peptide modification of the proximal DNA termini to facilitate metal-affinity coordination to the QD surface.[29] The benefits of this conjugation approach include the high affinity ($K_{eq} \sim 1 \times 10^9$ M^{-1}) and long-term stability of the interaction, the limited number of preparatory steps required (ratiometric mixing followed by rapid, spontaneous self-assembly), and the ability to generate conjugates where both valency and orientation can be controlled.[25,29–32]

Rather than using aniline-catalyzed chemoselective ligation to join the $(His)_6$-peptide to the DNA as done previously,[29,33] we implemented a linkage based on dithiol exchange as it requires fewer activation and

purification steps. This approach had already been confirmed to generate stable QD–DNA FRET conjugates.[21,34] More importantly, the disulfide linkage is significantly smaller than the hydrazone bond decreasing the size and spacing between the peptide and DNA moieties, which should also help restrict their freedom of movement once attached to the QD. Peptido–DNA chimeras were prepared as described in detail in the methods section and outlined in Figure 1B. The peptide sequence utilized here (C-GSGAAA-GLS-HHHHHH) consists of four functional modules as indicated. The C-terminal $(His)_6$ portion directly coordinates to the QD surface and does not provide for any lateral extension away from it.[31] The flexible GLS sequence is meant to allow the rest of the peptide to bend away from the QD surface and extend out in between the QDs surrounding PEG layer. The GSGAAA sequence acts as a linker extending through the PEG layer where the AAA sequence forms a short, partially rigid α-helix. Lastly, the N-terminal cysteine provides a thiol that is exploited as a unique site-specific chemical handle for attachment of thiolated DNA. Figure 1A shows a schematic of the QD–DNA construct with a single DNA wire on the surface. For the sake of clarity the wire is presented normal to the QD surface; however, despite the fact that the chemistry linking the DNA wires to the QD is fixed and smaller than the previous implementation, there will still be some steric freedom for the wire to adopt a variety of conformations with respect to the QD surface.[30] The fully assembled QD-photonic wire construct used in this study may be considered as a rigid DNA arm attached to the QD surface by an appended peptide with the greatest flexibility found at the intersection between the DNA and $(His)_6$-linker.

To provide insight into the ET kinetics and efficiencies along the DNA wires, three sets of QD-photonic wire constructs were analyzed where the distances between adjacent organic fluorophores were engineered to be approximately 0.5×, 1.0×, or 1.5 × R_0 of that donor–acceptor pair along each double stranded (ds) DNA wire, see Figure 1C and Supporting Information (SI) for the DNA sequences. Donor–acceptor spacings corresponding to 0.5×, 1.0×, or 1.5 × R_0 are expected to provide for estimated FRET efficiencies at each step of ∼98%, 50%, and 8%, respectively.[17] Although the QD to Cy3 spacing for the first ET step was inherently constrained by the peptide–DNA linkage chemistry, this approach allowed the remaining dyes to be systematically moved closer or further apart as a function of their donor–acceptor R_0. To achieve these designs, the 1.0 and 1.5 × R_0 constructs had the dyes assembled to a DNA template in a linear fashion, whereas in the 0.5 × R_0 assembly the DNA was hybridized in a concatenated manner. Within each of these constructs, the number of photonic wires attached to the central QD was also varied with the average number being 1, 2, 4, or 8 arms. In addition, every permutation of fluorophore combination was also constructed to obtain a complete picture of the influence of individual fluorophores on ET and especially on longer-range ET processes.

Spectral Overlap of QDs and the Multiple Organic Fluorophores. Previous work with a similarly arranged construct (QD-Cy3-Cy5-Cy5.5-Cy7) had shown that the terminal Cy7 dye functioned only as a terminal dark quencher.[29] Thus, ET efficiency in the last step could only be estimated from Cy5.5 donor PL loss as no sensitized emission was observed from the Cy7. To overcome this limitation while still maintaining four sequential ET steps, Cy3.5 was inserted between Cy3 and Cy5, and the problematic Cy7 dye was removed from the system. The absorption and emission spectra of the initial 525 nm emitting QD donor and the four cyanine fluorophores are shown in Figure 2A. This plot highlights the potential of this system to harness the energy of a photon, preferentially exciting the QD at ∼400 nm and transferring it to a spatially and spectrally separated terminal acceptor through four intermediary or FRET relay steps. The relevant photophysical parameters of each fluorophore are listed in Table 1 along with the calculated spectral overlap integrals, J, and the Förster distances, R_0, for each donor–acceptor pair. Values relevant for homoFRET between like cyanine dyes are also listed. The R_0 values for each FRET pair varied between ∼40 and 60 Å while J varied almost an order of magnitude from 1.3×10^{-13} to 1.4×10^{-12} cm^3 M^{-1}. Both parameters followed the expected trend of increasing as the donor emission and acceptor absorption spectral overlap improved. The values of J for each donor–acceptor pair are comparatively presented in Figure 2B and this overlay plot further highlights the optimized spectral characteristics of this system to transfer exciton energy sequentially over 300 nm of the visible spectrum using multiple ET steps. These overlap data also suggest that long-range spectral ET in which an intermediate dye is skipped over is unlikely to be significant. The one exception to the above is the relationship between the QD and Cy3.5, where the overlap integral is significant and the R_0 value is similar to the value between the QD and Cy3 (Table 1), 49 vs 46 Å (∼6% difference), respectively. Although J is ∼35% less than that of the QD and Cy3 pairing, there still remains the potential for energy to be transferred directly from the QD to Cy3.5 in constructs designed with shorter interfluorophore distance as in the 0.5 × R_0 assembly.

QD-Photonic Wires. We next examined in detail the FRET progression during the stepwise assembly of each of the QD-wire constructs with 1.5×, 1.0× and 0.5 × R_0 dye spacings. These were systematically built up to display an increasing average number of photonic wires (M) where M = 1, 2, 4, 8. Each of these constructs was also examined as sequential acceptors

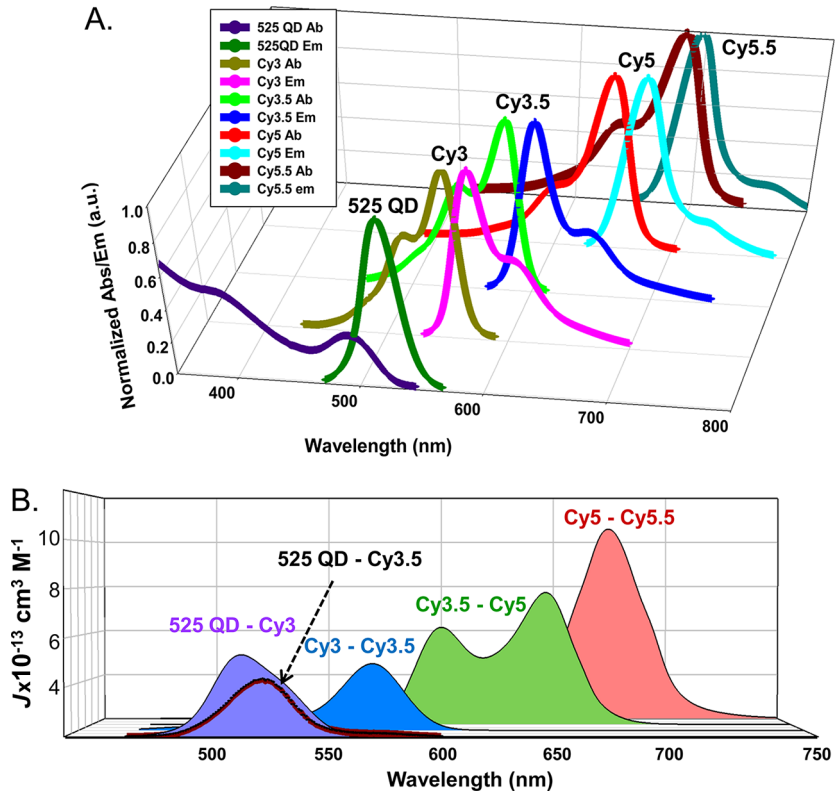

Figure 2. QD-dye spectral overlap. (A) Three-dimensional plot showing the absorption and emission of the 525 nm emitting QD along with the sequential donor/acceptor Cy3, Cy3.5, Cy5, and Cy5.5 cyanine dyes. (B) Calculated spectral overlap integral versus wavelength for the 525 QD-Cy3, Cy3-Cy3.5, Cy3.5-Cy5, and Cy5-Cy5.5 donor−acceptor pairs. The 525 QD-Cy3.5 pairing is also shown as indicated by the arrow.

TABLE 1. Photophysical and FRET Properties of the QDs and Fluorophores Used

					R_0 in Å/J in cm^3 M^{-1}[b]			
fluorophores	quantum yield	extinction coefficient (M^{-1}cm^{-1})	λ_{max} absorption	λ_{max} emission	Cy3	Cy3.5	Cy5	Cy5.5
525 nm QD	0.13[a]	213 0000 (at 400 nm)		523 nm	49/6.20e^{-13}	46/4.07e^{-13}	39/1.45e^{-13}	38/1.28e^{-13}
Cy3	0.15	150 000	550 nm	570 nm	47/3.96e^{-13}	47/4.16e^{-13}	46/3.45e^{-13}	41/1.99e^{-13}
Cy3.5	0.15	150 000	581 nm	596 nm		45/2.93e^{-13}	58/1.44e^{-12}	53/8.54e^{-13}
Cy5	0.28	250 000	649 nm	670 nm			59/8.81e^{-13}	61/1.10e^{-12}
Cy5.5	0.23	190 000	675 nm	694 nm				59/9.97e^{-13}

[a] QD quantum yield determined with dye in the full DNA assembly alone or with DNA assembled on QD. [b] R_0 and J values are averages calculated from the spectra of all dye-labeled DNA's used.

were added starting with only the initial QD donor and progressing to the full 4-dye QD-Cy3-Cy3.5-Cy5-Cy5.5 complex. All pertinent controls were also queried, including each dye alone within the full assembly (to estimate direct excitation contributions) and assemblies with one or more of the dyes missing. To develop a quantitative understanding of the underlying processes in terms of exciton transfer dynamics, we analyzed the data using two approaches: (1) an empirical analysis based on the collected data, and (2) a modeling approach based on applying Förster theory. The derivation of equations used and a detailed description of how these analyses were implemented can be found in the Materials and Methods, Data Analysis section; it is recommended that this description be read first in order to make the discussion below easier to follow. Because the empirical analysis operates more or less directly on the observed PL data, below we integrate it directly into our presentation of the data. The Förster analysis results are discussed immediately following.

PL Data and Empirical Analysis. For purposes of brevity, we provide only a representative discussion of the QD 1.5× and 1.0 × R_0 wire constructs (see Figure 3), and focus mainly on the 0.5 × R_0 wire constructs and on the initial QD-Cy3 distances as these are the most informative (see Figure 4 and Table 2). According to the empirical analysis, the donor energy loss and acceptor sensitization of each fluorophore at each QD:wire valence for all the systems were computed using the

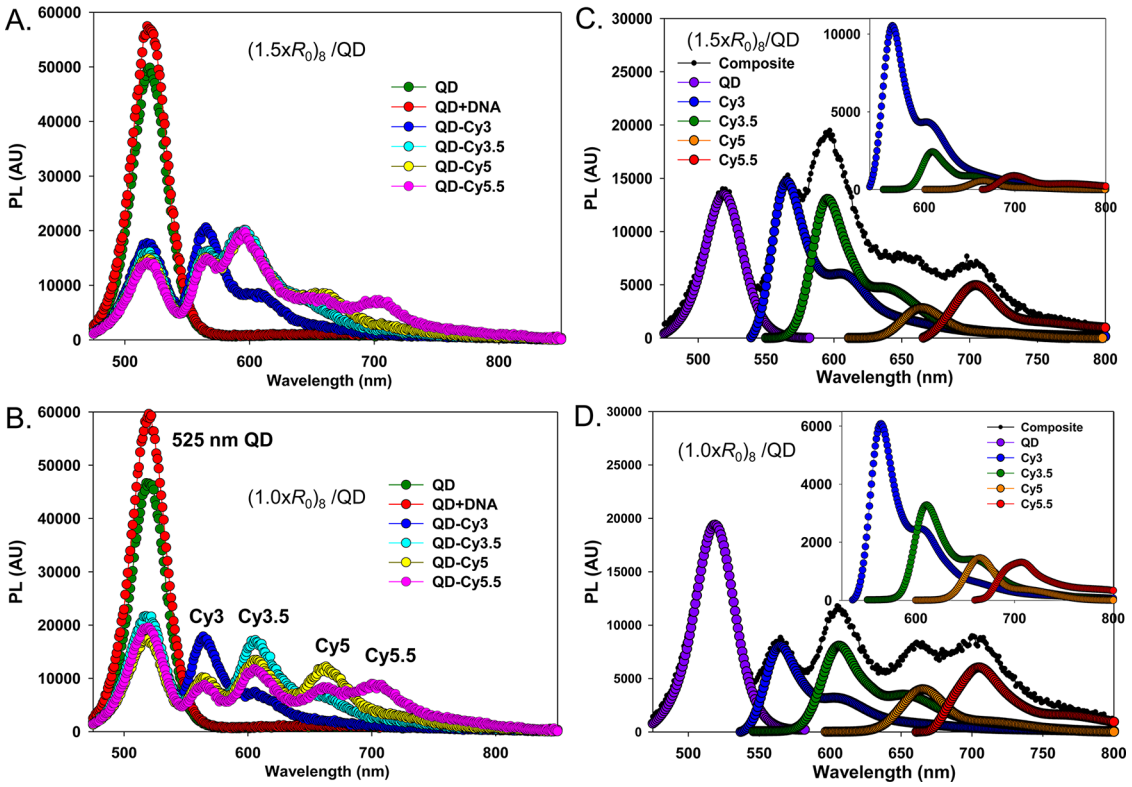

Figure 3. Emission profile and deconvolution of QD 1.5× and 1.0 × R_0 constructs with eight wires per QD. (A) Representative FRET progression of QD−DNA construct with eight photonic wires per QD and 1.5 × R_0 spacing between cyanine dyes. Green and red curves correspond to the emission spectrum of DHLA-PEG coated QDs and QDs with an average of eight dsDNA coupled to the surface, respectively. Subsequent curves show the intensity profile as the additional FRET acceptors are added. (B) Representative FRET progression of QD−DNA construct with eight photonic wires per QD and 1.0 × R_0 spacing between cyanine dyes. (C) Composite spectrum of full QD-Cy3-Cy3.5-Cy5-Cy5.5 construct with overlay of the deconvoluted contributions from each fluorophore for 1.5 × R_0 spacing and (D) 1.0 × R_0 spacing. Insets in C,D show the corresponding FRET-sensitized contributions for the Cy3 through Cy5.5 dyes. Excitation for all samples was at 400 nm.

empirical analysis eq 4,5 and are listed in the SI (Table S2). This table also includes data for control constructs in which individual dye(s) were removed. Selected data from all of these experiments are summarized in Table 2 as a function of assembly into the full QD-Cy3-Cy3.5-Cy5-Cy5.5 construct and the display valence around the QD. In addition to FRET from donor loss, the end-to-end exciton transfer efficiency, *E*, was also calculated using eq 3 as the ET steps increased concomitantly with the build up into the full QD-Cy3-Cy3.5-Cy5-Cy5.5 photonic wire. These latter values are listed parenthetically in Table 2.

The following discussion is organized according to the spacing between the dyes (0.5×, 1.0×, and 1.5 × R_0) with only the QD-Cy3 constructs treated separately, since the distance between these two initial chromophores was not intentionally varied in our experiments.

QD:Cy3 Constructs. Similar to what we have reported previously, we note a slight increase in QD PL when just the unlabeled DNA alone is assembled around the QD, see Figure 3A,B and 4A−D (compare red and green curves).[29,34,35] The magnitude of this change increases with the number of DNA wires conjugated to the QD. Such PL enhancement is believed to arise as a result of surface passivation effects following QD conjugation which reduces nonradiative recombination. This notion is supported by the fact that the ensemble QD excited state lifetime does not increase despite the increase in PL.[35,36] This enhancement is also accounted for in the analyses below.

Constructs with only two chromophore types present can be analyzed much more definitively than when more than two are involved. In particular, for the empirical analysis we can utilize the second equality in eq 10, taking the value of R_0 to be that given in Table 1 and deriving the Förster-weighted r_{ave} values (assuming the valence *M* to take its designed value). Such calculations find that the location of the Cy3 dye relative to the QD center varies. For example, the r_{ave} value in the four QD:(0.5 × R_0)$_m$ assemblies is estimated at 61.5 ± 0.3 Å or ~1.3 × R_0, and that for the QD:(1.5 × R_0)$_m$ constructs is remarkably similar at a 62.1 ± 1.4 Å separation, but the Förster-weighted spacing estimated for the four QD:(1.0 × R_0)$_m$ assemblies is 20% greater at 74.2 ± 9 Å or ~1.5 × R_0. For comparison purposes, our previous report had placed the initial Cy3 dye ~73 Å from the QD center.[29] As the (His)$_6$-peptide-dithiol linkage-DNA portion of the peptide−DNA composite is chemically identical in all three constructs, we ascribe this difference to the DNA

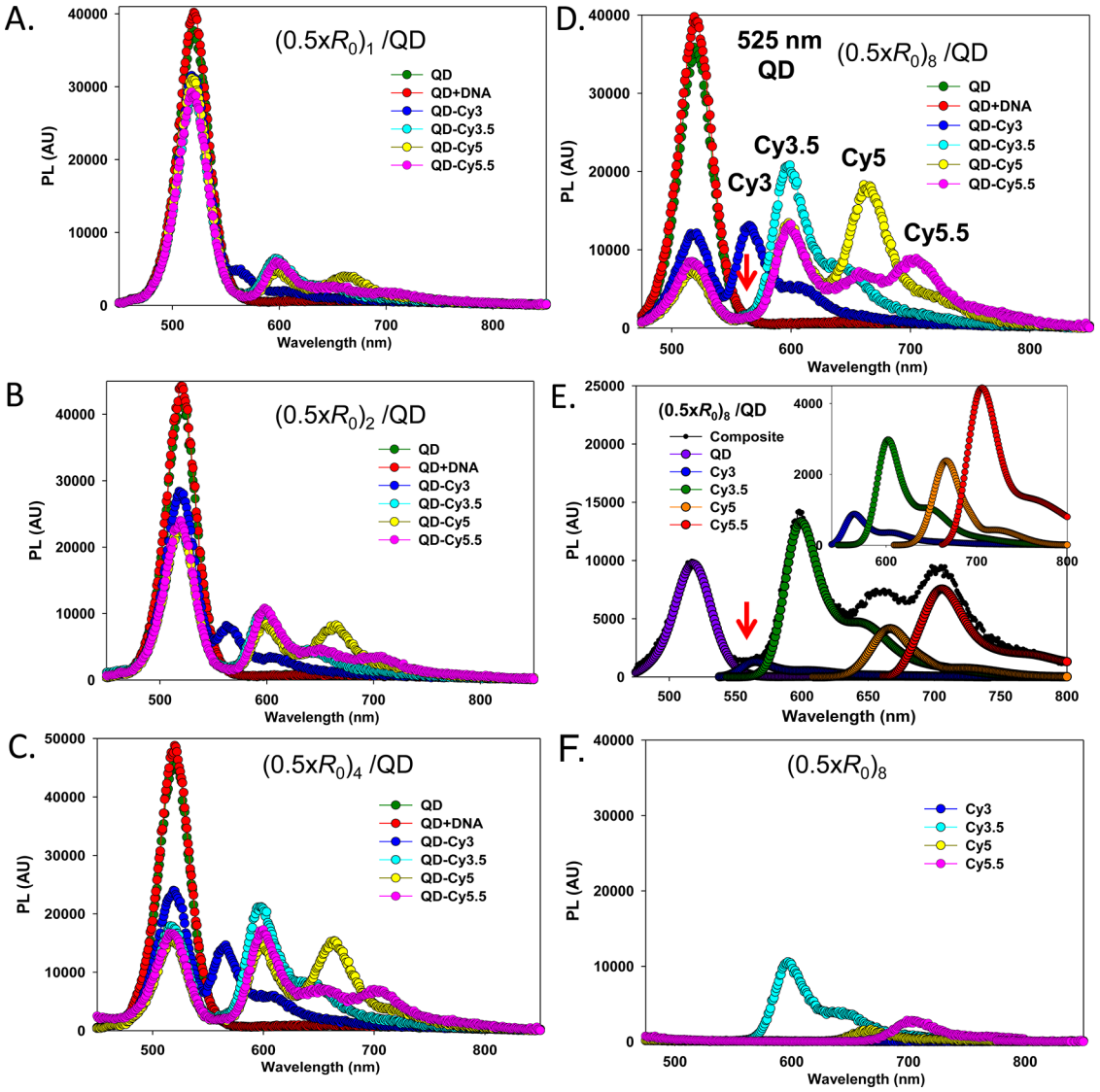

Figure 4. Fluorescent intensity profile of the 0.5 × R_0 QD photonic wire when assembled with increasing DNA wires. (A) Representative FRET progression of QD−DNA construct with 1 photonic wire per QD. Green and red curves correspond to the emission spectrum of DHLA-PEG coated QDs and QDs with an average of 1 dsDNA coupled to the surface, respectively. Subsequent curves show the intensity profile in the presence of additional FRET acceptors with 0.5 × R_0 spacing. (B) Representative FRET progression with an average of two dsDNA-wires coupled to the QD. (C) Representative FRET progression with an average of four dsDNA-wires coupled to the QD. (D) Representative FRET progression with an average of eight dsDNA-wires coupled to the QD. Excitation for all samples was at 400 nm. Note the decrease in QD PL and increase in Cy-dye sensitization as a function of the number of wires/QD. (E) Composite spectrum of full QD-Cy3-Cy3.5-Cy5-Cy5.5 8 dsDNA-wire construct in D with overlay of the deconvoluted contributions from each fluorophore. Inset shows the corresponding FRET-sensitized contributions for the Cy3 through Cy5.5 dyes. (F) Corresponding control emission spectra of each of the cyanine dyes individually assembled in the eight dsDNA-wires and directly excited at 400 nm.

sequence that is hybridized to the 1.0 × R_0 template and hypothesize that this may reflect some incomplete hybridization or "breathing" in the end portion of the DNA (see Figure 1C).[37,38] Alternatively, there may be some interactions between the Cy3 dye label on this DNA and the PEG layer that surrounds the QD during assembly. We do not assign this result to inefficient hybridization, as this complementary DNA pair had a relatively high T_m (~52 °C in 2.5X PBS) and hybridization was performed prior to QD assembly and appeared to be successful for all the other constructs. Although the initial design goal was for a near-equal FRET in the first step of the QD constructs, this difference does translate into a lower FRET rate for the first step in the QD:(1.0 × R_0)$_n$ system. We estimate that in the 1.0 × R_0 constructs, this first FRET step is ~50%, 50%, 30%, and 12% less efficient for the 1-, 2-, 4-, and 8-wire systems, respectively, than the average values noted for the 0.5× and 1.5 × R_0 assemblies, see Table 2. Nevertheless, the ability to increase the chances of an exciton reaching the first dye in this first step by increasing the discrete number of Cy3 dyes (i.e., wires) displayed around the QD remains intact and should increase the probability of energy flowing into the

TABLE 2. Estimated Donor Energy Losses and End-to-End Emission Efficiencies for Full QD-Dye Assemblies with Increasing Number of DNA-Wires Displayed: QD-(Cy3-Cy3.5-Cy5-Cy5.5)$_n$

	donor loss (end-to-end exciton transfer efficiency)				
assembly/no. of wires	QD	Cy3	Cy3.5	Cy5	Cy5.5
$(0.5 \times R_0)_m$					
$m = 1$	28%	93% (11%)	1% (14%)	93% (4%)	(1%)
2	47%	92% (20%)	0% (18%)	90% (7%)	(3%)
4	67%	94% (31%)	34% (32%)	90% (12%)	(5%)
8	79%	94% (40%)	77% (32%)	85% (19%)	(8%)
$(1.0 \times R_0)_m$					
$m = 1$	11%	62% (3%)	14% (1%)	13%(<1%)	(<1%)
2	19%	43% (5%)	53% (3%)	19% (<1%)	(1%)
4	38%	46% (13%)	45% (6%)	44% (<1%)	(2%)
8	68%	53% (37%)	58% (23%)	66% (5%)	(3%)
$(1.5 \times R_0)_m$					
$m = 1$	19%	24% (11%)	<1% (5%)	38% (1%)[a]	(<1%)
2	33%	25% (17%)	<1% (4%)	59% (<1%)[a]	(<1%)
4	47%	28% (24%)	<1% (3%)	65% (<1%)[a]	(<1%)
8	76%	29% (41%)	<1% (13%)	71% (2%)[a]	(2%)

[a] Reflects the quenching of directly excited Cy5 by Cy5.5 addition.

sequentially arrayed downstream acceptors. This last point is highlighted by examining the FRET efficiency for this first step across all the constructs. Although the efficiency displays some variation among the different constructs with values that range from 11 to 28% for 1-wire per QD, this still increases significantly up to 68−79% for 8-wires per QD (see Table 2).

QD:(1.5 × R_0)$_{1,2,4,8}$ Photonic Wires. Spectra for the 1-, 2-, and 4-wire constructs with a 1.5 × R_0 spacing between the adjacent cyanine dyes are shown along with their controls and the direct acceptor excitation components in the SI (Figures S7−S9). Donor energy loss and acceptor sensitization for each fluorophore at each QD:wire valence within this system as obtained from the empirical analysis are listed in Supporting Information, Tables S10−S13. The addition of successive dyes and its effect on the PL intensity of the 8-wire 1.5 × R_0 construct is shown in Figure 3A. The deconvolved spectra of each fluorophore within the full 8-wire QD-Cy3-Cy3.5-Cy5-Cy5.5 construct are shown in Figure 3C along with the sensitized fluorophore contribution in the inset. Following the interactions of the QD with the initial Cy3 dye, the QD is effectively quenched by the Cy3 dyes as wire valency/QD is increased (19%−76% for 1−8 wires, respectively) while Cy3 sensitization also increases proportionally (11%−41%) (see Table 2). Functioning as a donor, the Cy3 dye is only partially quenched by the Cy3.5 addition despite the increasing valency (average of ~27 ± 3%). In turn, the Cy3.5 dye does not appear to be quenched by the addition of the Cy5 acceptor nor is it significantly sensitized. In contrast, the Cy5 dye appears to be effectively quenched by the Cy5.5 addition, although end-to-end efficiency from the Cy3.5 onward is negligible. This apparent discrepancy arises from the fact that the Cy5 dye receives nontrivial direct excitation at 400 nm and it is this excitation that is then quenched by the proximal Cy5.5 acceptor due to the excellent spectral overlap of this pair. As expected for a <10% efficiency per step, tracking the percent difference in E between the QD-Cy3 construct and the full QD-Cy3-Cy3.5-Cy5-Cy5.5 construct reveals a decrease in overall exciton transfer efficiency approaching 100%, thus confirming the sharp drop in ET over four FRET pairs with the cyanine dyes spaced 1.5 × R_0 with respect to one another.

QD:(1.0 × R_0)$_{1,2,4,8}$ Photonic Wires. A second set of QD−DNA constructs was designed to have an average spacing of 1.0 × R_0 between the adjacent cyanine dyes. QDs were self-assembled with increasing wire valency as above and emission spectra collected with 400 nm excitation. Representative spectra for constructs with 1-, 2-, and 4 wires along with their controls and the direct acceptor excitation components are shown in the SI. Data from the stepwise assembly of the 8-branched structure is shown in Figure 3B along with the deconvolved and FRET sensitized components from the full QD-Cy3-Cy3.5-Cy5-Cy5.5 construct in Figure 3D. Discrete donor energy loss along with acceptor sensitization for each fluorophore at each QD:wire valence within this system is listed in the Supporting Information, Tables S6−S9.

The donor loss (E_D) appears to be linearly proportional to the number of wires with values increasing from 11% to 68% as the number of wires increased from 1 to 8 (Table 2). Interestingly, the E_D for Cy3 showed variability between 62% and 43% with no consistent trend observed versus the number of wires. The E_D values for Cy3.5 varied between 45% and 58% for the 2, 4, and 8-wire constructs, but had a value of

only 14% for the 1-wire construct. For Cy5, E_D increased from 13% to 66% for the 1, 2, 4, and 8-wire constructs. Overall terminal exciton transfer efficiency registers at <1% for the 1 wire system, but then, in contrast to the 1.5 × R_0 system described above, starts to steadily increase to 1%, 2%, and 3% as the average number of wires displayed around the QD increases from 1 up to 8. By increasing the number of wires around the QD, we are thus increasing the probability that a Cy3 dye will get excited and sensitize a full relay down the wire. A perfect 5-dye/4-FRET step functioning with a 1.0 × R_0 spacing for all participating dyes would be predicted to manifest a terminal exciton transfer efficiency of ~6−7% which is not inconsistent with our extrapolated values.

QD:(0.5 × R_0)$_{1,2,4,8}$ Photonic Wires. Figure 4A−D displays the FRET progression for the QD−DNA wire constructs with 0.5 × R_0 spacing as a function of the average number of photonic wires from 1 to 8. Each plot in Figure 4A−D also displays the change in fluorescent emission as the system is built up from just a QD to the full QD-Cy3-Cy3.5-Cy5-Cy5.5 complex. The composite spectrum for the full QD-Cy3-Cy3.5-Cy5-Cy5.5 8 dsDNA-wire construct of Figure 4D with overlay of the deconvoluted contributions from each fluorophore is shown in Figure 4E, with the inset showing the purely sensitized component. Figure 4F displays the direct excitation emission signature of control samples with 8 mol equiv of each fluorophore on the dsDNA and with no QD present, that is, direct excitation controls for the acceptor data in Figure 4D. These data reveal minimal direct excitation of the downstream fluorophores, with the exception being a small but significant excitation of Cy3.5. The most notable observation from the 1-, 2-, 4-, and 8-wire samples is the increase in ET flow through the system as the number of wires around each QD is increased. This change is manifest as a decrease in the PL intensity of the QD with a concomitant increase in the peak PL associated with the terminal cyanine dye in each construct. The 8-wire construct shown in Figure 4D shows clear sensitization of each acceptor (and decrease in previous donor emission) as successive dyes are added to the QD−DNA construct.

Several general trends may be noted in the data (Table 2). The E_D of the QDs increased nonlinearly from 28% to 79% as the number of photonic wires increased from 1 to 8. The E_D of Cy3 was independent of the number of wires with values ranging from 92 to 94%, reflecting a very efficient and almost quantitative FRET process, see red arrows in Figure 4D,E. Similar to the QDs, the E_D of Cy3.5 significantly increased from ~1% up to 77% as the number of wires was increased from 1 to 8. The E_D of Cy5 varied little with the number of wires on the QD surface (85% to 93%). These end-to-end exciton transfer efficiency (E) values show a common trend as the number of wires per QD was increased. The values of E for the QD-Cy3 complex increased nonlinearly from 11% to 40% and appeared to be approaching an asymptotic limit as the number of wires increased from 1 to 8. Similar values and trends for E were observed in the QD-Cy3-Cy3.5 complex, which increased from 14% to 32% over the same range of ratios. For the QD-Cy3-Cy3.5-Cy5 complex, the magnitude of E increased from 4% to 19% as the number of wires was increased. In the full construct, E ranged from ~1% to 8% as a function of the increasing number of wires. We note that the average E for the 1-wire construct was ~1% (values less than 1% are reported as such in Table 2), and thus the 8-fold increase in the average number of wires displayed around the QD resulted in an approximately 8-fold increase in the overall end-to-end efficiency. As expected, this system manifests the highest transfer efficiencies at each step and in the overall system.

Förster Analysis. For the Förster-based modeling analysis, we curve-fit some of the measured spectra using eq 6 with eqs 7−9, and then attempt to verify our understanding by making predictions regarding other measurements. As discussed in the Materials and Methods section and in the SI, we carry out this process starting from "ideal" simulations that utilize the photophysical parameters of Table 1. The basic geometry of the constructs is as shown in the schematic in Figure 5A and the simulations are performed over an ensemble of such structures in which the photonic wires are assumed to be straight but random in number (according to a Poisson distribution about the designed value), anchor point, and angle with respect to the QD, and with random orientations of the linkers anchoring the dyes to the wires. The outputs are predicted "ideal" spectra (or equivalently integrals of the individual peaks) to be compared with the observed PL data, with any differences then motivating "non-ideal" adjustments of the input parameters. The discussion is organized according to the number of different dyes added to the QD, with each step building on the previous one. In this development, we again emphasize the 0.5 × R_0 case which is generally the most informative since it has the strongest coupling and the PL is therefore dominated by the energy transfers of interest rather than by direct excitation. Most of the analysis results for the 1.0 × R_0 and 1.5 × R_0 cases are included in the SI.

QD:Cy3 Constructs. For the "ideal" simulations, all parameters are known except the scaled generation rate Ψ and the average QD-Cy3 distance r_{0i1}. We estimate these by fitting the QD and Cy3 emission peaks of a single spectrum; for example, in Figure 5B, we curve-fit the spectrum for the 0.5 × R_0 case with 2 Cy3 dyes (in blue) and obtain the good fit shown (in red) when the average QD-Cy3 distance r_{0i1} is taken to be about 67.6 Å (which implies the Cy3 dye sits about 15 Å outside the PEG layer). That this number is

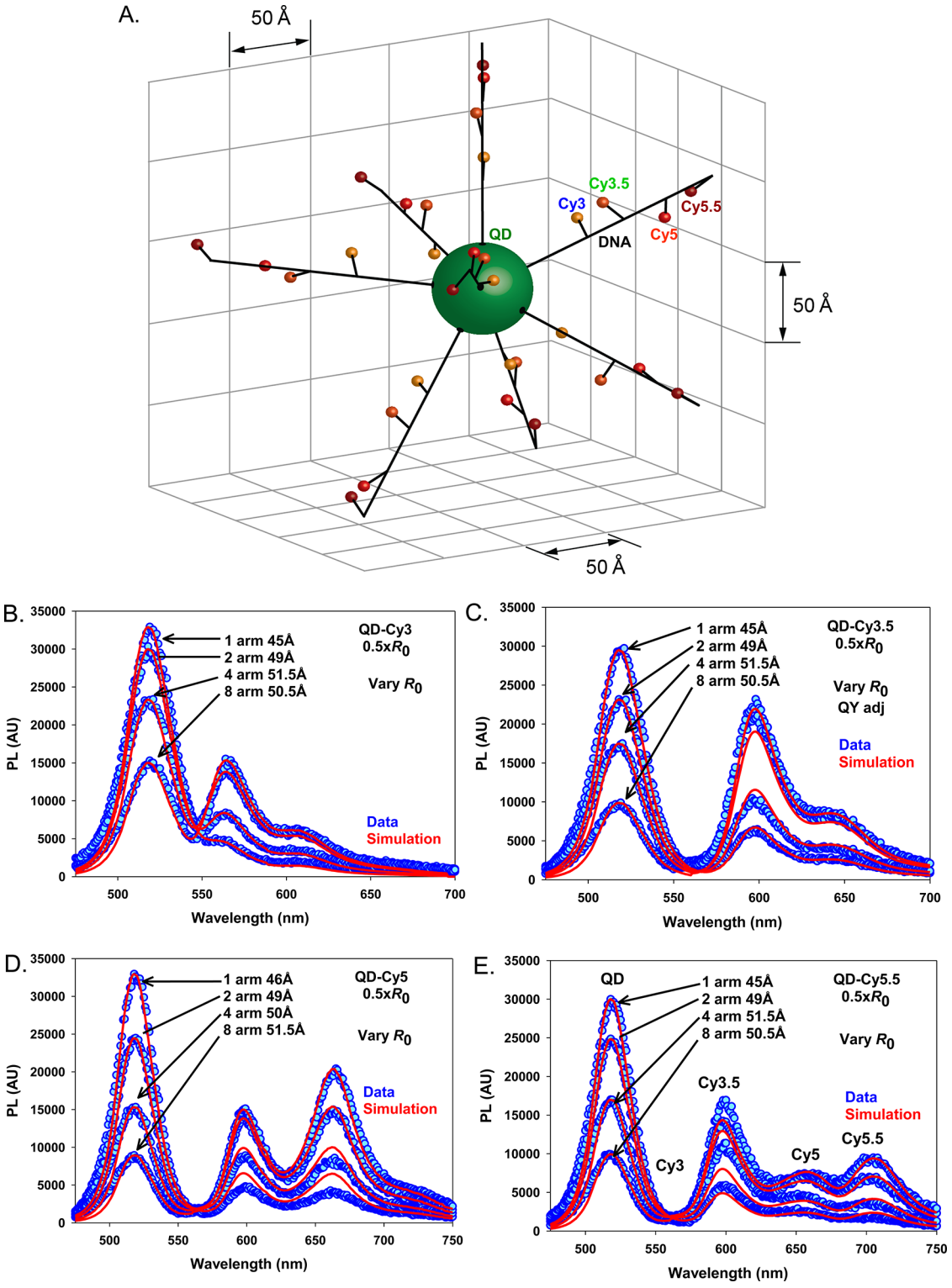

Figure 5. Simulating exciton transfer through the 0.5 × R_0 QD photonic wire assemblies. (A) Schematic showing how the position of the wires and the dyes on each wire were simulated using a Poisson approach to account for assembly heterogeneity and dye movement. (B) Plot showing the comparison between the 0.5 × R_0 QD-Cy3 PL emissions as an increasing number of DNA arms were assembled with the overlay of the simulated data. (C–E) Corresponding plots as in B for 0.5 × R_0 QD-Cy3.5, QD-Cy5, and QD-Cy5.5 assemblies, respectively. Adjustments made to R_0 or QY in the simulations are indicated.

larger than that deduced from the empirical analysis (61.5 Å) is likely due to the latter value being a Förster-weighted average that emphasizes constructs whose chromophores happen to be closer. Continuing with our analysis, we next use the parameters just determined from the 2-dye case to predict the spectra for

constructs with 1, 4, and 8 Cy3 dyes as shown in SI, Figure S10 (in red). Significant departures from experiment are observed, and as a possible explanation we observe that differing amounts of DNA in the QD coating will modify the local dielectric constant, and in turn raise R_0 according to eq 9 (*i.e.*, as $\Delta R_0 \cong -R_0\Delta\varepsilon_r/(3\varepsilon_r)$). Curve-fits allowing R_0 to vary give the results (for the $0.5 \times R_0$ case) shown in Figure 5B, with the simulations (in red) for all valences now agreeing well with experiment (in blue). That the required variations in R_0 are small and display the correct trend (*i.e.*, more DNA tends to require higher R_0) means that this explanation is plausible. The same treatment of the $1.5 \times R_0$ case yields very similar results (see SI Figure S11A); however, things work less well for the $1.0 \times R_0$ case (see Figure S11B) in that the required R_0 variation is considerably larger. In the discussion to follow we shall ignore the latter due to the other questions regarding this data (see "Note on QD:Cy3 Constructs" in the SI), and proceed as if the dielectric explanation were correct in all cases.

QD:Cy3-Cy3.5 Constructs. We next examine data for QD:Cy3-Cy3.5 constructs in which the dye spacing is $0.5 \times R_0$ and the FRET progression is followed as the average number of photonic wires (valence) is raised from $M = 1$ to 2 to 4 to 8. The predicted "ideal" simulations (including the adjusted R_0 values for the QD-Cy3 pair discussed earlier) are shown in SI, Figure S13 and qualitative agreement with the experimental data is obtained; however, there is a significant discrepancy in the *magnitude* of the Cy3.5 PL at ~600 nm. This discrepancy cannot be due to missing wires/dyes since the predicted peak is too *low*. Similarly, it seems unlikely to be explained by an error in the assumed Cy3.5 position or in the R_0 value for the Cy3−Cy3.5 pair since, unless the error is quite large, the Cy3.5 emission will continue to be dominated by the QD-Cy3 transfer. We are therefore led to suspect that the problem is in the "ideal" QY of the Cy3.5 dye given in Table 1. Adjusting the QY of the Cy3.5 dye from 0.15 to 0.24 yields the excellent agreement shown in Figure 5C (in red). A QY adjustment of this size is quite plausible based on the known sensitivity (*i.e.*, increase or decrease of QY) of quite closely related cyanine dyes to specific DNA sequences,[39,40] structural differences,[41,42] relative conformation,[43] solvation,[44] and a host of other environmental properties,[45,46] including proximity and binding to QD surfaces.[47] Other potential interacting and/or contributing factors may be the PEG layer surrounding the QDs and the high ionic strength of the buffer used here (~2.5× PBS). In a demonstrative example that may reflect these same issues, labeling maltose binding protein on an environmentally protected internal site with Cy3 dye allowed it to function as a near-unity or perfectly sensitized acceptor when attached to similar QD donors,[36] while labeling the exposed terminal of a peptide with this same dye acceptor dramatically reduced (>75%) its ability to be sensitized by the same QDs.[48] Most noteworthy in Figure 5C is that the predicted lack of Cy3 PL around 570 nm is indeed seen experimentally. This means that the close dye spacing results in a strong exciton transfer from the QD to the terminal Cy3.5 dyes with *near-100% efficiency*. This result is also evidence that, when the Cy3 dye is present/operative in a given wire, the Cy3.5 dye is essentially always there as well. Finally, the fact that this result is seen no matter the valence indicates that the photonic wires are acting largely independently.

It is important to mention that the QY values reported for each dye in Table 1 are those experimentally measured for each when those dyes alone are attached to the DNA. It is reasonable to use these as "ideal" values (Table 1), while realizing that they may differ from those appropriate when in the presence of the QD, the PEG layer, other dyes, and other structural effects.[39−47] As in the example of Cy3.5 above and in other cases below, when it seems plausible we suggest that deviations in the QY values could explain discrepancies between "ideal" simulations and experiment.

In SI, Figure S14A,B, we present spectral data (in blue) and model predictions (in red) for QD:Cy3-Cy3.5 constructs in which the dye spacings are $1.0 \times R_0$ and $1.5 \times R_0$. Again, curves are shown for photonic wire valences of 1, 2, 4, and 8, and for the simulations the parameters are those of Figures S11A,B. The agreement for $1.0 \times R_0$ in Figure S14A is excellent, while that for $1.5 \times R_0$ in Figure S14B is reasonably good. Regarding the latter, small adjustments of specific parameters could be used to achieve better agreement, but this strategy is not pursued here because distinguishing between real photophysical corrections and curve fitting would be challenging. Lastly, it should be noted that the simulations in Figures S14A,B are direct predictions analogous to Figure S13 and do not include enhancing the Cy3.5 QY as was done in Figure 5C; hence if the QY modification for the $0.5 \times R_0$ case is physical, it must arise from a host of complex interrelated effects that arise at the QD−DNA−dye interface as discussed above.

QD:Cy3-Cy3.5-Cy5 and QD:Cy3-Cy3.5-Cy5-Cy5.5 Constructs. For the QD-wire constructs containing 3 and 4 dyes per photonic wire, we again start by examining cases when the dye-to-dye spacing is $0.5 \times R_0$. Figure 5 panels D,E show PL spectra (blue) for the QD-wire constructs with 3 and 4 dyes per wire, respectively, and with average wire valencies of 1, 2, 4, and 8. The Förster predictions for these cases appear in SI, Figures S6A and S6B with all parameters kept as earlier (including enhancing the QY of the Cy3.5 as done for Figure 5C) except that the QD peaks are again fit to account for small changes in the normalization. Most noteworthy in these plots is that, as in Figure 5C, simulation again predicts a complete lack of PL from

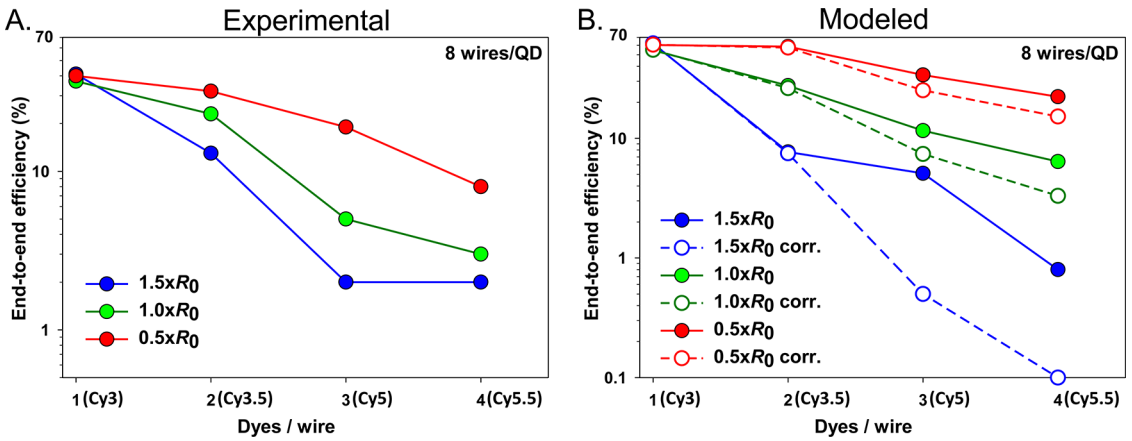

Figure 6. Comparison of estimated and modeled exciton transfer efficiency through the QD photonic wire assemblies. (A) Plot tracking end-to-end exciton transfer efficiencies (as a percentage, log scale) versus sequential dye assembly measured within each of the 1.5×, 1.0×, and 0.5 × R_0 QD assemblies. Dyes/wire: 1 = Cy3; 2 = Cy3-Cy3.5; 3 = Cy3-Cy3.5-Cy5; 4 = Cy3-Cy3.5-Cy5-Cy5.5. (B) Plot tracking the end-to-end exciton transfer efficiencies (as a percentage, log scale) *versus* sequential dye assembly as modeled within each of the 1.5, 1.0, and 0.5 × R_0 QD assemblies. Corrected (corr.) data accounts for the direct excitation of dyes other than the initial QD donor.

the intermediate dyes (due to the expected high transfer efficiency); however, this time the prediction is *not borne out by experiment* except for the Cy3 dye. Clearly, the explanation must involve some mechanism that raises the PL of the intermediate dyes and lowers it for the terminal dyes. One possibility is that the spacings between the dyes are larger than expected. While the flexible linkers allow some variation in these spacings, simulations show that the changes required to produce spectra like those seen experimentally are much larger than is plausible. Similarly, it could be that the QY of the intermediate dyes are higher and the terminal dyes are lower than their ideal values, but, again, the required changes appear to be much larger than is plausible. Still another possible mechanism would be that the Cy5 and/or Cy5.5 dyes are either absent due to incomplete structure formation or inactive due photobleaching, self-quenching, or other such related phenomena. Indeed, there is much evidence in the literature regarding the subpar performance of Cy5 as a FRET acceptor or donor. In particular, when attached to DNA, Cy5 has performed as a quasi "dark quencher" that has demonstrated a very low rate of sensitized emission, especially in the context of QD donors.[34,49,50] Additionally, the fact that Cy5 is known to photobleach/inactivate *via* a number of mechanisms, including free radical interaction with photoexcited dyes,[51−55] suggests that this could indeed be a significant contributor to this issue.

To model absent/inactive dyes, we simply incorporate probabilities for their deactivation within our overall statistical approach. For the simulation results in Figure 5D,E (red) we have adjusted these probabilities so as to allow the simulated PL spectra to match experiment for the 3- and 4-dye constructs. Good agreement is seen in the 3-dye case (Figure 5D) when the probability of the Cy5 dye being present/active is 35% (and Cy3.5 QY is raised from 0.25 to 0.30 and that of the Cy5 from 0.28 to 0.38). For the 4-dye case, the reasonable agreement seen in Figure 5E is obtained when the probability of the Cy5 dye being present/active is further reduced to 20% and that of the Cy5.5 is set at 50%. The levels of nonexisting/inactive dyes in these two cases are obviously quite high and we believe this reflects the magnitude of this issue within this DNA construct. Although we vary both assembly efficiency and dye activity as parameters to match the experimental data, we hypothesize that the primary culprit in this format may be dye performance since our previous work[29] and fast protein liquid chromatography (FPLC), analysis of similar DNA structures suggest that hybridization/assembly is ≥80% efficient (*i.e.*, ≥ 80% of the DNA structures are properly formed; data not shown).

Next we consider the 3 and 4 dye constructs in which the dye-to-dye spacings are 1.0 × R_0 and 1.5 × R_0. These cases are less informative because their relatively poor transfer efficiency means that the PL of the outer dyes is dominated by direct excitation. The plots comparing experiment and simulation appear in Supporting Information, Figures S16A and S16C (1.0 × R_0, 3- and 4-dye) and in Figures S16B and S16D (1.5 × R_0, 3- and 4-dye). For the simulations, the probabilities of the outer dyes being present/active are used as fitting parameters, and the results are generally reasonably good. It is worth noting that the levels of nonexisting/inactive outer dyes is significantly lower than it is in the 0.5 × R_0 case, a result that is perhaps consistent with a photobleaching mechanism in which available free radicals act on *excited* dyes, and so can be expected to weaken as the dye spacings increase.

End-to-End Exciton Transfer. The end-to-end exciton transfer efficiency E can be estimated using eq 3 with the terms in that formula obtained from either the empirical or the Förster analysis. In general, these

estimates will be flawed in not properly accounting for direct excitation, that is, they will include excitons generated at intermediate dyes that make it to the terminal dye as contributing to the overall E. A key advantage of the Förster analysis is that one can correct for this error by performing simulations in which the direct excitation terms are turned off (except for the QD contribution), and thereby obtain a corrected end-to-end efficiency that we have termed $\hat{E}$. The detailed picture provided by the Förster analysis also gives us an understanding of the calculated efficiencies and how they can be improved.

As a representative data set, we focus on QD-photonic wire constructs having an average of 8 wires per QD and varying both the number of dyes per wire and the dye spacing. The end-to-end efficiencies calculated for these constructs are summarized in Figure 6 with estimates derived from the empirical analysis in Figure 6A and from the Förster analysis in Figure 6B. The latter plot includes both the efficiency E (solid lines) and the corrected efficiency $\hat{E}$ (dashed lines) that has the error associated with direct excitation eliminated. The uncorrected efficiencies derived by the two methods are in rough agreement and follow expectation. In particular, the efficiency is essentially independent of the dye spacing when only Cy3 is present, and then it declines as more dyes are added and especially when dye spacing is large. As discussed earlier, for a dye spacing of $0.5 \times R_0$ the E is unchanged (*i.e.*, dominated by the QD-Cy3 transfer since that spacing is $\sim 1.3 \times R_0$,) when the Cy3.5 dye is added, but when subsequent dyes are included the efficiency shows a substantial drop. According to the analysis given in the previous section, this latter decline is associated with a significant fraction of the Cy5 and Cy5.5 dyes being absent or inactive. When the dye spacing is increased to $1.0 \times R_0$ or $1.5 \times R_0$ the efficiencies drop off rapidly as the number of exciton transfer steps increases and their probability decreases.

Comparing the corrected and uncorrected curves in Figure 6B, we find that the effect of the direct excitation error on the foregoing conclusions is solely quantitative. The correction is largest for wires with three and four dyes because the Cy3.5 dye has the strongest direct excitation. Additionally, the relative size of the correction increases with dye spacing because in these cases the transfer is weakest and it is direct excitation that accounts for most of the measured terminal PL. As a result, for a spacing of $1.5 \times R_0$ the E for the full four-dye construct may only be about 0.1% as opposed to the uncorrected estimate of about 1%.

CONCLUSIONS

We have explored issues related to the design and construction of DNA-based QD-photonic wire constructs for delivering absorbed photon energy from the central QD out to the periphery using multistep FRET over a range $\geq$15 nm (QD core to Cy5.5) and $\geq$30 nm if one considers the fully formed structures.[29] The DNA-guided assembly method provides considerable flexibility for positioning of the fluorophores and this feature can be used to optimize the overall harvesting capacity and efficiency of the structures. As our first generation structure had almost the same architecture,[29] there are many similarities between that system and the construct described here. Both consisted of a central QD with sequentially arranged dyes attached on a DNA sequence extending out from the QD which provided the central energy harvesting capability. In terms of the first QD-to-Cy3 step, both the previous and current constructs demonstrated an efficiency in the range of 70−80% depending upon the number of arms displayed around the QD. However, as the earlier effort barely achieved a putative end-to-end efficiency of <0.1% through the same number of four FRET steps and over a similar distance ($\geq$15 nm), we reengineered four key aspects of the composite structure in this work: (1) making the DNA modification chemistry smaller, (2) optimizing donor−acceptor dye pairings, (3) varying donor−acceptor dye spacing as a function of R_0, and (4) increasing the number of distinct DNA wires displayed around each central QD donor. These changes led to almost 2 orders of magnitude improvement in the exciton transfer efficiency to the final terminal dyes with an overall E through the optimized, cascaded five-fluorophore/four ET step system that approached 10%.

In addition to an empirical analysis of the data, we carried out a detailed analysis using Förster theory with various sources of randomness accounted for by averaging over ensembles of modeled constructs. Fits to the spectra suggest near-ideal behavior when the photonic wires have two sequential acceptor dyes (Cy3 and Cy3.5) and exciton transfer efficiencies approaching 100% are seen when dye spacings are $0.5 \times R_0$. However, as additional dyes are included in each wire, the efficiency drops substantially, an effect that appears to arise from the poor photophysical performance of the last two acceptor dyes (Cy5 and Cy5.5). On the basis of this interpretation we conclude that even higher efficiency FRET relays (assuming a similar architecture) should be readily achievable if (i) the initial QD-Cy3 spacing can be decreased, and (ii) the problem of inactive dyes can be avoided, by implementing known methods for blocking dye degradation,[55] and/or by switching to other more-stable/photophysically robust dye families. Derivative architectures that provide multiple potential acceptors for each donor, thus increasing the probability of FRET, may also prove beneficial. With these improvements and with dye spacings of $0.5 \times R_0$, or less, it should become possible to approach theoretical transfer efficiencies above 90% in photonic wires involving four or more FRET steps.

The ability to achieve high exciton transfer efficiencies over multiple steps and over relatively long nanoscale distances (0.10 μm) suggests that hybrid energy harvesting/photonic wire structures such as those highlighted here may have much to offer for research into artificial photosynthesis.[56] Indeed, one exciting idea is to use the DNA wire portion to couple multiple QDs around an artificial or harvested reaction center for charge separation. The physical DNA length combined with its persistence length can allow multiple QDs to be spatially arranged around such a center while the high rate of FRET simultaneously provides for consistent and efficient exciton delivery. Another alternative would be to incorporate electroactive compounds such as Ru- or Os-metal chelates directly onto the DNA itself.[57,58] Along with starting to achieve high exciton transfer efficiencies, another critical benefit to this research approach arises directly from the DNA chemistry itself, namely the intrinsic reliance on self-assembly which provides the ability to rapidly reconfigure any construct while still achieving exquisite positional control without requiring any complex *de novo* synthesis.[57] Overall, the lessons learned from designing and optimizing these QD-based photonic structures can contribute important insight toward the development of efficient light-harvesting and light-energy exploiting devices.

MATERIALS AND METHODS

Quantum Dots. CdSe–ZnS core–shell QDs with a PL maximum centered at ~523 nm (referred to as 525 nm QDs for simplicity) were synthesized using a high temperature reaction of organometallic precursors in hot coordinating solvents as described previously.[59,60] The native QDs were cap-exchanged with dihydrolipoic acid appended with polyethylene glycol (PEG, MW ~750) that terminated in a methoxy group (DHLA-PEG ligands); see the SI for the chemical structure.[61] These ligands provide for robust QDs that are stable in water for long periods of time over wide ranges of pH and ionic strength.

DNA Sequences, Dye-Labels, and Ligation to Modified Peptides. The DNA oligonucleotides in these experiments were *de novo* designed synthetic sequences that were purchased from Integrated DNA Technologies (Coralville, IA), with the exception of the Cy3.5-labeled strands, which were purchased from Operon Biotechnologies, Inc. (Huntsville, AL); see Supporting Information (SI, Table S1) for specific sequences and predicted melt temperatures (T_m). The DNA sequences were designed such that the interdye spacings were proportional to ~0.5, 1.0, or 1.5 times the R_0 value for each specific dye pair. The length of the six carbon dye linker as well as the relative angular separation of the dyes on the DNA helix were also taken into account when making these determinations. For the 1.0 × R_0 and 1.5 × R_0 systems, a single contiguous template, obtained with a terminal 3′-protected thiol, was used to assemble complementary oligonucleotides A″–D″ (1.5 × R_0) or A′–D′ (1.0 × R_0), which contained a uniquely placed Cy3, Cy3.5, Cy5, or Cy5.5 dye, or were left unlabeled. The 0.5 × R_0 system required the use of a staggered or concatenated DNA construction (*i.e.*, with no template) to afford the correct spacing for oligonucleotides A–D, where each was again purchased with its specific dye label or left unlabeled. Strand models for the different R_0 structures are shown in Figure 1B.

For assembling the DNA to the QDs, thiolated oligonucleotides were attached to hexahistidine-appended, $(His)_6$, peptides to provide for metal-affinity coordination to the QD surface. Peptide Ac-CGSGAAAGLS$(H)_6$-$CONH_2$ was obtained from Bio-Synthesis (Lewisville, Texas), where Ac is an acetyl group protecting the N-terminal primary amine and $CONH_2$ is an amide group protecting the C-terminal carboxylic acid. The terminal thiols on the cysteine residues were then activated with pyridine disulfide (Sigma-Aldrich; St. Louis, MO) to form a pyridyl disulfide that then underwent thiol-exchange with the DNA which had been prereduced with tris(2-carboxyethyl)-phosphine (TCEP, Sigma) to form a peptido–DNA chimera as described in ref 21, see Figure 1B. For the peptide ligation of the 0.5 × R_0 construct, oligonucleotide B was obtained with a 3′-protected thiol in addition to the dye label. Peptide-modified DNAs were purified, desalted, and quantitated using UV–visible absorption, dried down, and stored at −20 °C until resolubilized for use as described.[21,62]

Hybridization and Self-Assembly of the QD–DNA Photonic Wires. For each of the configurations described here, an aliquot of the $(His)_6$-peptide-modified DNA template was resolubilized in 2.5× phosphate buffered saline (PBS: 342.5 mM NaCl, 25 mM phosphate, 6.75 mM KCl) to make a 20 μM stock solution. This stock was then mixed together with dye-labeled or unlabeled complementary DNA oligonucleotides at the desired molar ratios in a 500 μL Eppendorf tube, denatured in a water bath at 100 °C for 5 min, allowed to cool to 25 °C, and then kept at 4 °C for 30 min. Unlabeled segments were always included as necessary to maintain the DNA construct in its full double-stranded form. The ratio of each unlabeled or dye-labeled DNA segment to each other was always maintained at 1:1 (equimolar amounts) within each of the structures assembled. The hybridized DNA constructs were then assembled onto the QDs in 2.5X PBS for 1–2 h at room temperature (RT). This procedure yielded 100 μL volumes of self-assembled QD–DNA conjugates where the QD concentration was maintained fixed at 0.30 μM and the number or ratio of surrounding photonic wires displayed on each QD was varied as described.[29]

Data Collection. Fluorescence spectra from each of the ensemble conjugate samples were collected on a Tecan Safire Dual Monochromator Multifunction Microtiter Plate Reader (Tecan, Research Triangle Park, NC) using 400 nm excitation. Data was collected from triplicate experiments and representative spectra are shown here and in the SI (Figures S2–S9). Solutions examined include the QD–DNA bioconjugates and control samples of QD, DNA, with dyes only, and QD–DNA–bioconjugates with selected dyes removed.[21,29]

Data Analysis. Data obtained from the various QD–DNA constructs were analyzed using two approaches, one being the standard empirical approach used by us[29] and others,[63] and the other based on Förster theory.[64,65] The overall purpose of these analyses is to interpret the PL data obtained for the various QD–DNA constructs, and thereby to attain an understanding of their photophysical behavior, to estimate and compare their exciton transfer efficiencies, and to provide a solid basis for further improving their performance in future work.

A foundational assumption of both analyses is that our samples are optically thin (*i.e.*, dilute) so that the fluorophores of a given construct do not interfere with one another. This assumption allows the overall spectrum $G(\lambda)$ of a given construct (in numbers of emitted photons collected per unit wavelength per second) to be resolved as

$$G(\lambda) = f_0(\lambda)\Phi_0 + \sum_{j=1}^{N} f_j(\lambda)\Phi_j \quad (1)$$

where the $f_j(\lambda)$ are the normalized emission spectra of the QDs ($j = 0$) and of the N different dyes in the construct ($j = 1, ..., N \leq 4$ for this work), and the Φ_j represent the number of emitted photons collected per second from each chromophore. For use below, it is also helpful to measure the spectra $G_j(\lambda)$ of molar

equivalents of the different chromophores on an individual basis. Analogous to eq 1, these spectra obey

$$G_j(\lambda) = f_j(\lambda)\Phi_j^0 \tag{2}$$

where Φ_j^0 are the number of emitted photons collected per second from the chromophore of type j when no other chromophores are present. If desired, one can convert from numbers of emitted photons to numbers of excited chromophores using the QY; specifically, the numbers of excited chromophores (of type j) per second for the two cases just discussed are Φ_j/Q_j and Φ_j^0/Q_j, respectively, where Q_j is the fluorescence QY of chromophore of type j.

Empirical Analysis. For this approach a numerical deconvolution of eq 1 is performed to estimate the values of Φ_j. This was accomplished using the Multipeak Fitting tool in Igor Pro (version 6.1) in a manner similar to that described in ref 66. In addition, values for Φ_j^0 were extracted from control experiments using eq 2. The end-to-end exciton transfer efficiency (E) of each construct was then estimated using[29,63]

$$E = \frac{(\Phi_N - \Phi_N^0)/Q_N}{\Phi_0^0/Q_0} \tag{3}$$

where the denominator is the number of excited QDs (per second) and the numerator is the number of excited terminal dyes (per second) that did not become excited as a result of direct excitation. Equation 3 thus gauges the end-to-end efficiency so long as direct excitations of dyes situated between the QD donor and the terminal acceptor are negligible. It should also be noted that, to calculate E from the extracted Φ_j and Φ_j^0 using eq 3, the QYs of the QD and the terminal dye (under the experimental conditions) must be known *a priori*.

Two other standard measures of efficiency are the average FRET donor efficiency and the sensitized acceptor emission efficiency, respectively:[64]

$$E_D = 1 - \Phi_D/\Phi_D^0 \qquad E_A = 1 - \Phi_A/\Phi_A^0 \tag{4,5}$$

These formulas are typically employed when the system consists of a simple donor−acceptor dye pair, but for larger structures it is also possible for them to have meaning. For example, E_D will be a measure of the efficiency of transfer from a "donor" D (which can be multiple dyes of the same type) to an "acceptor" A (which can be multiple dyes of possibly even different types) if Φ_D and Φ_D^0 are integrals of the donor spectra (as deconvolved from full spectra) obtained with and without the acceptor being present, respectively. In the empirical analysis of the data, these formulas are applied to the deconvolved emission peak areas (derived in the manner described earlier) in order to estimate the transfer efficiencies of individual steps in a FRET cascade. It is important to note that "efficiencies" so calculated will lose meaning if there are contributions from fluorophores other than the PL of A to D that are affected by the presence or absence of A; see the SI for further discussion.

Förster Analysis. For this approach, we analyze the data using detailed models of the constructs assuming they obey Förster theory, that is, with the chromophores interacting solely *via* point dipole−dipole coupling. Because we are interested only in steady-state measurements, a solution of identical constructs will be governed by the following linear algebra (see the SI for the derivation):

$$W_{ij}\left[1 + \sum_{m=1}^{M}\sum_{n=j}^{N} b_{ijmn}\right] - \sum_{m=1}^{M}\sum_{n=1}^{j} b_{mnij}W_{mn} = \eta_j + a_{ij}\frac{1 - M\sum_{n=1}^{N}\eta_n}{1 + \sum_{m=1}^{M}\sum_{n=1}^{N} a_{mn}} \qquad \begin{matrix} i = 1, \ldots, M \\ j = 1, \ldots, N \end{matrix} \tag{6}$$

where W_{ij} are the (normalized) time-integrated probabilities that a dye of type j on photonic wire i will be excited, η_j is the probability of direct excitation of a dye of type j, and the a_{ij} and b_{ijmn} are the normalized QD−dye and dye−dye coupling matrices, respectively. To connect with experiment, the integrated probabilities in the foregoing equations must be related to the PL areas Φ_i and Φ_i^0 appearing in eq 1 and eq 2, which again give the collected energy emitted per second by chromophores of type i in the constructs (in the presence or absence of the other chromophores, respectively). In terms of the quantities in eq 6, the emission spectra from the different chromophores will be given by $\Psi Q_0 W_0 f_0(\lambda)$, for the QD, and $\Psi Q_j W_{ij} f_j(\lambda)$, for the dyes, where $\Psi \equiv \rho L \Omega \varphi$ is the scaled generation rate, φ is the number of excitons per second generated in each construct (which depends on the extinction coefficient, the intensity, and the quantum efficiency), ρ is the concentration of constructs, L is the path length, and Ω expresses the fraction of the emitted radiation that enters the detector. It follows that

$$\Phi_0 = \Psi Q_0 W_0 \quad \Phi_0^0 = \Psi Q_0 \eta_0 \quad \Phi_j = \Psi Q_j \sum_{i=1}^{M} W_{ij}$$

$$\Phi_j^0 = \Psi Q_j M \eta_j \tag{7}$$

In principle, by using eq 6 with eq 7 to fit experimental data, one could estimate the values of the coupling coefficients and thereby obtain a basic characterization of the system. Alternatively, such a fitting could be interpreted as yielding a geometrical characterization since according to Förster theory the coupling coefficients obey

$$a_{ij} = \left(\frac{R_0^{0j}}{r_{0ij}}\right)^6 \qquad b_{ijmn} = \left(\frac{R_0^{in}}{r_{ijmn}}\right)^6 \tag{8}$$

where the R_0^{ij} are the Förster distances characterizing the transfer between a donor chromophore of type i and an acceptor chromophore of type j, and r_{0ij} and r_{ijmn} are the QD-dye and dye−dye distances, respectively. The Förster distances are readily computed from the known donor emission spectra, acceptor absorption spectra, and the molar extinction coefficients using[64]

$$R_0 = 9780\left(\frac{\kappa^2 Q_D J}{n^4}\right)^{1/6} \tag{9}$$

where J is the spectral overlap integral for the donor−acceptor pair, n is the refractive index of the medium, Q_D is the fluorescence QY of the donor, and κ^2 is the dipole orientation factor. A value of $\kappa^2 = {}^2/_3$ is appropriate for the random dipole orientations encountered in these randomly assembled systems.[22] As discussed below, the accuracy of R_0 values may be limited due to uncertainties in QY or refractive index, and such uncertainties would obviously affect the accuracy of any dimensional characterization.

Equation 6 and eq 7 are for a solution of identical constructs, and to deal with various structural variations seen in real samples we employ a statistical approach in which the observables are estimated by ensemble averages. The model constructs are of the form shown in Figure 5A,[56,65] with possible variations in the number of wires in the constructs (as a result of the method of assembly), in the positions of their anchor points on the QDs, in the positions of the dyes on the wires (as a result of their flexible linkers), in the angles of the wires with respect to the QD (with the greatest flexibility found at the intersection between the DNA and $(His)_6$-linker),[30] in which specific dyes are absent/inactive as result of an incomplete conjugate assembly, incomplete wire assembly and/or a number of photophysical issues such as photobleaching or other effects arising from incorporation into a DNA scaffold. For initial simulations we make the following "ideal" assumptions: (1) the QYs and R_0 values are as given in Table 1; (2) the DNA templated wires are directed at random angles; (3) the wires are anchored to the QD at *random* positions; (4) the numbers of wires are Poisson distributed about the designed average; (5) the dye positions

along the DNA templates are at distances $0.5 \times R_0$, $1.0 \times R_0$, or $1.5 \times R_0$ with a linker displacement of 15 Å in a *random* direction; and (6) the structures are completely formed with all dyes present. In the simplest situation involving only the QD donor and the Cy3 acceptor dyes, the foregoing analysis simplifies greatly, and the efficiency measure E_D, in eq 4,5 becomes:

$$E_D = \left\langle \frac{R_0^6 \sum_{i=1}^{M} (1/r_{0i1})^6}{1 + R_0^6 \sum_{i=1}^{M} (1/r_{0i1})^6} \right\rangle = \frac{MR_0^6}{MR_0^6 + r_{ave}^6} \qquad (10)$$

where the angle brackets represent the ensemble average, R_0 is the Forster distance for the QD-Cy3 pair, and the second equality defines a Förster-weighted average distance r_{ave} between the chromophores. Obtaining the latter in this way represents the use of FRET as a "spectroscopic ruler,"[67] a process that is relatively unambiguous only because of the simplicity of the two-chromophore situation. In more general situations, the simulations are performed by generating an ensemble of structures, solving eq 6 with eqs 1,7,8,9 to obtain the emission spectra for each subpopulation, and then computing the ensemble average. Some aspects of such simulated spectra are curve-fit to data to obtain certain parameters, and the remainder are then regarded as predictions to be compared with experiment. Deviations inevitably occur, and we then look to explain these using hypotheses built around possible violations of one or more of the "ideal" assumptions. This approach allows us to posit plausible explanations for the experimental observations.

Finally, once a plausible interpretation has been reached, we then turn to the analysis of performance and to estimating the efficiency with which the constructs transfer excitons. The easiest approach is simply to use the relations in eq 7 to compute the E defined in eq 3 directly, and possibly also the efficiencies defined in eq 4,5. However, a better procedure is to perform additional calculations in which all the parameter values of the model are kept fixed except the direct excitation parameters η_i. By assuming only the QD is excited, we can then use eq 3 to compute the end-to-end efficiency without the aforementioned error introduced by direct excitation of intermediate dyes. We call this quantity the corrected end-to-end efficiency, $\hat{E}$.

Conflict of Interest: The authors declare no competing financial interest.

Acknowledgment. The authors acknowledge the Office of Naval Research, the NRL NSI, and DTRA JSTO MIPR No. B112582M for financial support. W.R.A. is grateful to NSERC for a postdoctoral fellowship.

Supporting Information Available: DHLA-ligand structure, derivation of the Förster formalism used, control data, and selected methods along with further discussion of results. This material is available free of charge via the Internet at http://pubs.acs.org.

Note Added after ASAP Publication: Due to a production error, this paper was published on the Web on 7/11/2013 with an error in Table 2. The correct version was reposted on 7/17/2013.

REFERENCES AND NOTES

1. Fu, J. L.; Liu, M. H.; Liu, Y.; Yan, H. Spatially-Interactive Biomolecular Networks Organized by Nucleic Acid Nanostructures. *Acc. Chem. Res.* **2012**, *45*, 1215–1226.
2. Michelotti, N.; Johnson-Buck, A.; Manzo, A. J.; Walter, N. G. Beyond DNA Origami: the Unfolding Prospects of Nucleic Acid Nanotechnology. *Wiley Interdisc. Rev. Nanomed. Nanobiotechnol.* **2011**, *4*, 139–152.
3. Pinheiro, A. V.; Han, D. R.; Shih, W. M.; Yan, H. Challenges and Opportunities for Structural DNA Nanotechnology. *Nat. Nanotechnol.* **2012**, *6*, 763–772.
4. Wilner, O. I.; Willner, I. Functionalized DNA Nanostructures. *Chem. Rev.* **2012**, *112*, 2528–2556.
5. Graugnard, E.; Kellis, D. L.; Bui, H.; Barnes, S.; Kuang, W.; Lee, J.; Hughes, W. L.; Knowlton, W. B.; Yurke, B. DNA-Controlled Excitonic Switches. *Nano Lett.* **2012**, *12*, 2117–2122.
6. Teo, Y. N.; Kool, E. T. DNA-Multichromophore Systems. *Chem. Rev.* **2012**, *112*, 4221–4245.
7. Wei, B.; Dai, M. J.; Yin, P. Complex Shapes Self-Assembled from Single-Stranded DNA Tiles. *Nature* **2012**, *485*, 623–626.
8. McKee, M. L.; Milnes, P. J.; Bath, J.; Stulz, E.; O'Reilly, R. K.; Turberfield, A. J. Programmable One-Pot Multistep Organic Synthesis Using DNA Junctions. *J. Am. Chem. Soc.* **2012**, *134*, 1446–1449.
9. Lin, C. X.; Jungmann, R.; Leifer, A. M.; Li, C.; Levner, D.; Church, G. M.; Shih, W. M.; Yin, P. Submicrometre Geometrically Encoded Fluorescent Barcodes Self-Assembled from DNA. *Nat. Chem.* **2012**, *4*, 832–839.
10. Wang, T.; Sha, R. J.; Dreyfus, R.; Leunissen, M. E.; Maass, C.; Pine, D. J.; Chaikin, P. M.; Seeman, N. C. Self-Replication of Information-Bearing Nanoscale Patterns. *Nature* **2011**, *478*, 225–228.
11. Castro, C. E.; Kilchherr, F.; Kim, D. N.; Shiao, E. L.; Wauer, T.; Wortmann, P.; Bathe, M.; Dietz, H. A Primer to Scaffolded DNA Origami. *Nat. Meth.* **2011**, *8*, 221–229.
12. Dutta, P. K.; Varghese, R.; Nangreave, J.; Lin, S.; Yan, H.; Liu, Y. DNA-Directed Artificial Light-Harvesting Antenna. *J. Am. Chem. Soc.* **2011**, *133*, 11985–11993.
13. Rothemund, P. W. K. Folding DNA to Create Nanoscale Shapes and Patterns. *Nature* **2006**, *440*, 297–302.
14. Seeman, N. C. An Overview of Structural DNA Technology. *Mol. Biotechnol.* **2007**, *37*, 246–257.
15. Albinsson, B. Energy Transfer On the Right Path. *Nat. Chem.* **2011**, *3*, 269–270.
16. Garo, F.; Haner, R. A DNA-Based Light-Harvesting Antenna. *Angew. Chem. Int. Ed.* **2012**, *51*, 916–919.
17. Sapsford, K. E.; Berti, L.; Medintz, I. L. Materials for Fluorescence Resonance Energy Transfer Analysis: Beyond Traditional Donor-Acceptor Combinations. *Angew. Chem. Int. Ed.* **2006**, *45*, 4562–4588.
18. Kuzyk, A.; Schreiber, R.; Fan, Z. Y.; Pardatscher, G.; Roller, E. M.; Hogele, A.; Simmel, F. C.; Govorov, A. O.; Liedl, T. DNA-Based Self-Assembly of Chiral Plasmonic Nanostructures with Tailored Optical Response. *Nature* **2012**, *483*, 311–314.
19. Shen, X. B.; Song, C.; Wang, J. Y.; Shi, D. W.; Wang, Z. A.; Liu, N.; Ding, B. Q. Rolling Up Gold Nanoparticle-Dressed DNA Origami into Three-Dimensional Plasmonic Chiral Nanostructures. *J. Am. Chem. Soc.* **2012**, *134*, 146–149.
20. Stein, I. H.; Steinhauer, C.; Tinnefeld, P. Single-Molecule Four-Color FRET Visualizes Energy-Transfer Paths on DNA Origami. *J. Am. Chem. Soc.* **2011**, *133*, 4193–4195.
21. Algar, W. R.; Wegner, D.; Huston, A. L.; Blanco-Canosa, J. B.; Stewart, M. H.; Armstrong, A.; Dawson, P. E.; Hildebrandt, N.; Medintz, I. L. Quantum Dots as Simultaneous Acceptors and Donors in Time-Gated Forster Resonance Energy Transfer Relays: Characterization and Biosensing. *J. Am. Chem. Soc.* **2012**, *134*, 1876–1891.
22. Medintz, I. L.; Mattoussi, H. Quantum Dot-Based Resonance Energy Transfer and Its Growing Application in Biology. *Phys. Chem. Chem. Phys.* **2009**, *11*, 17–45.
23. Algar, W. R.; Susumu, K.; Delehanty, J. B.; Medintz, I. L. Semiconductor Quantum Dots in Bioanalysis: Crossing the Valley of Death. *Anal. Chem.* **2011**, *83*, 8826–8837.
24. Ko, S. H.; Du, K.; Liddle, A. Quantum-Dot Fluorescence Lifetime Engineering with DNA Origami Constructs. *Angew. Chem. Int. Ed.* **2013**, *52*, 1193–1197.
25. Sapsford, K. E.; Algar, W. R.; Berti, L.; Boeneman Gemmill, K.; Casey, B. J.; Oh, E.; Stewart, M. H.; Medintz, I. L. Functionalizing Nanoparticles with Biological Molecules: Developing Chemistries that Facilitate Nanotechnology. *Chem. Rev.* **2013**, *113*, 1904–2074.
26. Lu, H.; Schops, O.; Woggon, U.; Niemeyer, C. M. Self-Assembled Donor Comprising Quantum Dots and Fluorescent Proteins for Long-Range Fluorescence Resonance Energy Transfer. *J. Am. Chem. Soc.* **2008**, *130*, 4815–4827.
27. Woller, J. G.; Hannestad, J. K.; Albinsson, B. Self-Assembled Nanoscale DNA–Porphyrin Complex for Artificial Light-Harvesting. *J. Am. Chem. Soc.* **2013**, *135*, 2759–2768.

28. Tikhomirov, G.; Hoogland, S.; Lee, P. E.; Fischer, A.; Sargent, E. H.; Kelley, S. O. DNA-Based Programming of Quantum Dot Valency, Self-Assembly and Luminescence. *Nat. Nanotechnol.* **2011**, *6*, 485–490.
29. Boeneman, K.; Prasuhn, D. E.; Blanco-Canosa, J. B.; Dawson, P. E.; Melinger, J. S.; Ancona, M.; Stewart, M. H.; Susumu, K.; Huston, A.; Medintz, I. L. Self-Assembled Quantum Dot-Sensitized Multivalent DNA Photonic Wires. *J. Am. Chem. Soc.* **2010**, *132*, 18177–18190.
30. Boeneman, K.; Deschamps, J. R.; Buckhout-White, S.; Prasuhn, D. E.; Blanco-Canosa, J. B.; Dawson, P. E.; Stewart, M. H.; Susumu, K.; Goldman, E. R.; Ancona, M.; et al. Quantum Dot DNA Bioconjugates: Attachment Chemistry Strongly Influences the Resulting Composite Architecture. *ACS Nano* **2010**, *4*, 7253–7266.
31. Sapsford, K. E.; Pons, T.; Medintz, I. L.; Higashiya, S.; Brunel, F. M.; Dawson, P. E.; Mattoussi, H. Kinetics of Metal-Affinity Driven Self-Assembly between Proteins or Peptides and CdSe–ZnS Quantum Dots. *J. Phys. Chem. C* **2007**, *111*, 11528–11538.
32. Medintz, I. L.; Konnert, J. H.; Clapp, A. R.; Stanish, I.; Twigg, M. E.; Mattoussi, H.; Mauro, J. M.; Deschamps, J. R. A Fluorescence Resonance Energy Transfer Derived Structure of a Quantum Dot-Protein Bioconjugate Nanoassembly. *Proc. Natl. Acad. Sci. U.S.A.* **2004**, *101*, 9612–9617.
33. Prasuhn, D. E.; Deschamps, J. R.; Susumu, K.; Stewart, M. A.; Boeneman, K.; Blanco-Canosa, J. B.; Dawson, P. E.; Medintz, I. L. Polyvalent Display and Packing of Peptides and Proteins on Semiconductor Quantum Dots: Predicted *versus* Experimental Results. *Small* **2009**, *6*, 555–564.
34. Medintz, I. L.; Berti, L.; Pons, T.; Grimes, A. F.; English, D. S.; Alessandrini, A.; Facci, P.; Mattoussi, H. A Reactive Peptidic Linker for Self-Assembling Hybrid Quantum Dot–DNA Bioconjugates. *Nano Lett.* **2007**, *7*, 1741–1748.
35. Medintz, I. L.; Clapp, A. R.; Mattoussi, H.; Goldman, E. R.; Fisher, B. R.; Mauro, J. M. Self-Assembled Nanoscale Biosensors Based on Quantum Dot FRET Donors. *Nat. Mater.* **2003**, *2*, 630–638.
36. Clapp, A. R.; Medintz, I. L.; Mauro, J. M.; Fisher, B. R.; Bawendi, M. G.; Mattoussi, H. Fluorescence Resonance Energy Transfer between Quantum Dot Donors and Dye-Labeled Protein Acceptors. *J. Am. Chem. Soc.* **2004**, *126*, 301–310.
37. Sulaiman, A.; Zen, F. P.; Alatas, H.; Handoko, L. T. Dynamics of DNA Breathing in the Peyrard-Bishop Model with Damping and External Force. *Phys. D, Nonlin. Phenom.* **2012**, *241*, 1640–1647.
38. Zeida, A.; Machado, M. R.; Dans, P. D.; Pantano, S. Breathing, Bubbling, and Bending: DNA Flexibility from Multimicrosecond Simulations. *Phys. Rev. E* **2012**, *86*, 021903.
39. Agbavwe, C.; Somoza, M. M. Sequence-Dependent Fluorescence of Cyanine Dyes on Microarrays. *PLOS One* **2011**, *6*, e22177.
40. Akimkin, T. M.; Tatikolov, A. S.; Yarmoluk, S. M. Spectral and Fluorescent Study of the Interaction of Cyanine Dyes Cyan 2 and Cyan 45 with DNA. *High Energy Chem.* **2011**, *45*, 222–228.
41. Renikuntla, B. R.; Rose, H. C.; Eldo, J.; Waggoner, A. S.; Armitage, B. A. Improved Photostability and Fluorescence Properties through Polyfluorination of a Cyanine Dye. *Org. Lett.* **2004**, *6*, 909–912.
42. Chibisov, A. K. Photonics of Dimers of Cyanine dyes. *High Energy Chem.* **2007**, *41*, 200–209.
43. Levitus, M.; Ranjit, S. Cyanine Dyes in Biophysical Research: The Photophysics of Polymethine Fluorescent Dyes in Biomolecular Environments. *Q. Rev. Biophys.* **2011**, *44*, 123–151.
44. Petrov, N. K.; Gulakov, M. N.; Alfimov, M. V.; Busse, G.; Techert, S. Solvation-Shell Effect on the Cyanine-Dye Fluorescence in Binary Liquid Mixtures. *J. Res. Phys. Chem. Chem. Phys.* **2007**, *221*, 537–547.
45. Muddana, H. S.; Morgan, T. T.; Adair, J. H.; Butler, P. J. Photophysics of Cy3-Encapsulated Calcium Phosphate Nanoparticles. *Nano Lett.* **2009**, *9*, 1559–1566.
46. Cao, J. F.; Wu, T.; Hu, C.; Liu, T.; Sun, W.; Fan, J. L.; Peng, X. J. The Nature of the Different Environmental Sensitivity of Symmetrical and Unsymmetrical Cyanine Dyes: An Experimental and Theoretical Study. *Phys. Chem. Chem. Phys.* **2012**, *14*, 13702–13708.
47. McArthur, E. A.; Godbe, J. M.; Tice, D. B.; Weiss, E. A. A Study of the Binding of Cyanine Dyes to Colloidal Quantum Dots Using Spectral Signatures of Dye Aggregation. *J. Phys. Chem. C* **2012**, *116*, 6136–6142.
48. Medintz, I. L.; Clapp, A. R.; Brunel, F. M.; Tiefenbrunn, T.; Uyeda, H. T.; Chang, E. L.; Deschamps, J. R.; Dawson, P. E.; Mattoussi, H. Proteolytic Activity Monitored by Fluorescence Resonance Energy Transfer Through Quantum-Dot–Peptide Conjugates. *Nat. Mater.* **2006**, *5*, 581–589.
49. Zhang, C. Y.; Hu, J. Single Quantum Dot-Based Nanosensor for Multiple DNA Detection. *Anal. Chem.* **2010**, *82*, 1921–1927.
50. Zhang, C. Y.; Johnson, L. W. Quantum-Dot-Based Nanosensor for RRE IIB RNA-Rev Peptide Interaction Assay. *J. Am. Chem. Soc.* **2006**, *128*, 5324–5325.
51. Freeman, L. M.; Armani, A. M. Photobleaching of Cy5 Conjugated Lipid Bilayers Determined with Optical Microresonators. *IEEE J. Sel. Top. Quantum Electron.* **2012**, *18*, 1160–1165.
52. Fureder-Kitzmuller, E.; Hesse, J.; Ebner, A.; Gruber, H. J.; Schutz, G. J. Non-Exponential Bleaching of Single Bioconjugated Cy5 Molecules. *Chem. Phys. Lett.* **2005**, *404*, 13–18.
53. Berlier, J. E.; Rothe, A.; Buller, G.; Bradford, J.; Gray, D. R.; Filanoski, B. J.; Telford, W. G.; Yue, S.; Liu, J. X.; et al. Quantitative Comparison of Long-Wavelength Alexa Fluor dyes to Cy Dyes: Fluorescence of the Dyes and their Bioconjugates. *J. Histochem. Cytochem.* **2003**, *51*, 1699–1712.
54. Frederix, P.; de Beer, E. L.; Hamelink, W.; Gerritsen, H. C. Dynamic Monte Carlo Simulations to Model FRET and Photobleaching in Systems with Multiple Donor–Acceptor Interactions. *J. Phys. Chem. B* **2002**, *106*, 6793–6801.
55. Altman, R. B.; Terry, D. S.; Zhou, Z.; Zheng, Q. S.; Geggier, P.; Kolster, R. A.; Zhao, Y. F.; Javitch, J. A.; Warren, J. D.; Blanchard, S. C. Cyanine Fluorophore Derivatives with Enhanced Photostability. *Nat. Methods* **2012**, *9*, 68–71.
56. Albinsson, B.; Hannestad, J.K.; Börjesson, K. Functionalized DNA Nanostructures for Light Harvesting and Charge Separation. *Coord. Chem. Rev.* **2012**, *256*, 2399–2413.
57. Stewart, M. H.; Huston, A.; Scott, A. L.; Efros, A.; Melinger, J.; Boeneman Gemmill, K.; Trammell, S.; Blanco-Canosa, J.; Dawson, P. E.; Medintz, I. L. Complex Förster Energy Transfer Interactions between Semiconductor Quantum Dots and a Redox-Active Osmium Assembly. *ACS Nano* **2012**, *6*, 5330–5347.
58. Medintz, I. L.; Pons, T.; Trammell, S.; Grimes, A.; English, D.; Blanco-Canosa, J.; Dawson, P.; Mattoussi, H. Interactions between Redox Complexes and Semiconductor Quantum Dots Coupled *via* a Peptide Bridge. *J. Am. Chem. Soc.* **2008**, *130*, 16745–16756.
59. Dabbousi, B. O.; Rodriguez-Viejo, J.; Mikulec, F. V.; Heine, J. R.; Mattoussi, H.; Ober, R.; Jensen, K. F.; Bawendi, M. G. (CdSe)ZnS Core-Shell Quantum Dots: Synthesis and Optical and Structural Characterization of a Size Series of Highly Luminescent Materials. *J. Phys. Chem. B* **1997**, *101*, 9463–9475.
60. Peng, Z. A.; Peng, X. Formation of High-Quality CdTe, CdSe, and CdS Nanocrystals Using CdO as Precursor. *J. Am. Chem. Soc.* **2001**, *123*, 183–184.
61. Mei, B. C.; Susumu, K.; Medintz, I. L.; Delehanty, J. B.; Mountziaris, T. J.; Mattoussi, H. Modular Poly(ethylene glycol) Ligands for Biocompatible Semiconductor and Gold Nanocrystals with Extended pH and Ionic Stability. *J. Mater. Chem.* **2008**, *18*, 4949–4958.
62. Sapsford, K. E.; Farrell, D.; Sun, S.; Rasooly, A.; Mattoussi, H.; Medintz, I. L. Monitoring of Enzymatic Proteolysis on a Electroluminescent-CCD Microchip Platform using Quantum Dot-Peptide Substrates. *Sens. Actuator B, Chem.* **2008**, *139*, 13–21.
63. Hannestad, J. K.; Sandin, P.; Albinsson, B. Self-Assembled DNA Photonic Wire for Long-Range Energy Transfer. *J. Am. Chem. Soc.* **2008**, *130*, 15889–15895.
64. Lakowicz, J. R. *Principles of Fluorescence Spectroscopy*, 3rd ed.; Springer: New York, 2006.

65. Van Patten, P. G.; Shreve, A. P.; Lindsey, J. S.; Donohoe, R. J. Energy-Transfer Modeling for the Rational Design of Multiporphyrin Light-Harvesting Arrays. *J. Phys. Chem. B* **1998**, *102*, 4209–4216.
66. Medintz, I. L.; Farrell, D.; Susumu, K.; Trammell, S. A.; Deschamps, J. R.; Brunel, F. M.; Dawson, P. E.; Mattoussi, H. Multiplex Charge Transfer Interactions between Quantum Dots and Peptide-Bridged Ruthenium Complexes. *Anal. Chem.* **2009**, *81*, 4831–4839.
67. Stryer, L.; Haugland, R. P. Energy Transfer: A Spectroscopic Ruler. *Proc. Natl. Acad. Sci. U.S.A.* **1968**, *58*, 719–726.